SOURCE
DATA

TRANSPARENT
PROCESS

Glutamate dehydrogenase1 supports HIF-1α stability to promote colorectal tumorigenesis under hypoxia

Kunhua Hu[1,†] (ID), Yufeng Ding[2,†] (ID), Hongwen Zhu[3,†] (ID), Xiaoqian Jing[4,†], Weiling He[5,*], Hua Yu[2,**] (ID) & Xiongjun Wang[2,***] (ID)

Abstract

Tumor cells surviving hypoxic stress acquire the ability to drive cancer progression. To explore the contribution of dehydrogenases to the low oxygen concentration response, we used siRNAs targeting 163 dehydrogenase-coding genes and discovered that glutamate dehydrogenase 1 (GDH1) plays a critical role in regulating colorectal cancer (CRC) cell survival under hypoxia. We observed that GDH1 deficiency had an inhibitory effect on CRC occurrence and impaired hypoxia-inducible factor 1-alpha (HIF-1α) stability even under hypoxia. Mechanistically, hypoxia triggered p300 recruitment to GDH1, promoting its acetylation at K503 and K527. GDH1 acetylation at K527 induced the formation of a GDH1 complex with EGLN1/HIF-1α; in contrast, GDH1 acetylation at K503 reinforced its affinity for α-ketoglutarate (αKG), and glutamate production. In line with this view, αKG is a product of GDH1 under normoxia, but hypoxia stimulation reversed GDH1 enzyme activity and αKG consumption by the EGLN1/HIF-1α complex, increasing HIF-1α stability and promoting CRC progression. Clinically, hypoxia-modulated GDH1 AcK503/527 can be used as a biomarker of CRC progression and is a potential target for CRC treatment.

Introduction

When the stress signal of extracellular oxygen exhaustion is transduced to intracellular EGLN1, a process of stress called hypoxia occurs. Tumor cells that survive hypoxia acquire the ability to metastasize, resist drugs, or tolerate nutrient limitation. However, how tumor cells survive in response to hypoxia is still unclear. Upon hypoxia, HIF1α is reported to be stabilized and accumulated in various cancer cells and is associated with the progression and adverse clinical outcome of many different tumor types, including colorectal cancer (CRC) (Brahimi-Horn *et al*, 2007; Böğürcü *et al*, 2018). Hence, discovery of a potential strategy to modulate the tumor cell response to hypoxia would be of great significance.

The activity of EGLN1 is tightly associated with HIF1α stability and is affected by the EGLN1 substrate oxygen and cofactor αKG. αKG is not only an intermediate metabolite in the Krebs cycle but also a direct product of glutamate metabolism (Stillman *et al*, 1993). Multiple enzymes are involved in αKG metabolism. For example, glutamic-oxaloacetate transaminase (GOT) and members of the glutamic-pyruvic transaminase (GPT) family produce αKG via glutamate deamination or a transaminase reaction. Members of the GDH family produce αKG via glutamate dehydrogenation, while members of the isocitrate dehydrogenase (IDH) family produce αKG via isocitrate dehydrogenation. In glioma cells, the absence of GDH1 was found to reduce the cellular level of αKG by approximately 65%, indicating that GDH1 might play a major role in αKG production in glioma cells (Yang *et al*, 2009). However, there is no clear association between αKG and CRC progression under hypoxia.

Generally, αKG is maintained at a steady state within the cell (Wang *et al*, 2019b), but dramatic changes in intracellular αKG levels profoundly impact gene transcription and signal transduction. Given that αKG is a cofactor for dioxygenases, such as TETs, KDMs, and EGLNs, it is reasonable to question whether changes in intracellular αKG levels can alter the activities of these enzymes. For example, the absence of BCAT1 was shown to cause αKG to accumulate to twice its basal level, and this increase in αKG activated EGLN1, which in turn inhibited the stability of HIF1α (Raffel *et al*, 2017).

---

1   Guangdong Key Laboratory of Liver Disease Research, The Third Affiliated Hospital of Sun Yat-Sen University, Guangzhou, China
2   School of Life Sciences, Precise Genome Engineering Center, Guangzhou University, Guangzhou, China
3   Department of Analytical Chemistry and CAS Key Laboratory of Receptor Research, Shanghai Institute of Materia Medica, Chinese Academy of Sciences, Shanghai, China
4   Department of General Surgery, Ruijin Hospital, Shanghai Jiao Tong University School of Medicine, Shanghai, China
5   The First Affiliated Hospital of Sun Yat-Sen University, Guangzhou, China
    *Corresponding author. Tel: +86-020-87755766; E-mail: hewling@mail.sysu.edu.cn
    **Corresponding author. Tel: +86-020-86236055; E-mail: yuhua@sibcb.ac.cn
    ***Corresponding author. Tel: +86-020-86236055; E-mail: xiongjunwang@sibs.ac.cn; wangxiongjun@gzhu.edu.cn
    †These authors contributed equally to this work

However, the *Km* value of EGLN1 for αKG is 1.3 μM (Lorenzo *et al*, 2014), and the intracellular αKG concentration varies from approximately 10–200 μM depending on the cell context (Jin *et al*, 2015). Also, a prolyl hydroxylases *in vitro* assay showed 2-Hydroxyglutarate (2HG) could activate EGLN1 (Tarhonskaya *et al*, 2014) probably because 2HG has a similar structure with αKG and meanwhile *in vitro* assay facilitated the enriched 2HG to bind EGLN1. Therefore, we suspect that the global change in αKG concentration induced by BCAT1 or other αKG-producing or -consuming enzymes should be insufficient to affect the enzyme activity of EGLN1 by exchanging of αKG/2HG.

In this study, we found that once cells suffer hypoxia stress, GDH1 targets the EGLN1/HIF1α complex after GDH1 acetylation by p300. In detail, AcK527 induced the formation of the GDH1/EGLN1/HIF1α axis, while GDH1 acetylation at K503 alleviated the restriction of αKG binding to GDH1, AcK503-GDH1 resulted in glutamate production using αKG as substrate. As a consequence of the combined GDH1 acetylation at K503 and K527, the reversed GDH1 activity likely consumed αKG around the GDH1/EGLN1/HIF1α complex, which led to the inhibition of EGLN1 activity and in turn stabilized HIF1α. Of note, the synchronic acetylation of GDH1-K503/K527 can be used as a biomarker of CRC progression, and thus, blockade of AcK503/527-GDH1 would benefit CRC treatment.

Results

GDH1 is required for the response to hypoxia and is associated with a poor prognosis in CRC

To discover the contribution of tumor metabolism, especially dehydrogenases, to the hypoxia response, we screened 163 dehydrogenase-coding genes under hypoxia and observed that GDH1 depletion dramatically induced cell death under hypoxia (Fig 1A). We depleted GDH1 in HCT116 and SW480 cells (Fig EV1A) and found that CRC cells lacking GDH1 were more sensitive to hypoxia than those expressing GDH1, while loss of GDH1 slightly reduced cell proliferation under normoxic conditions (Fig EV1B). In addition, compared with the control cells, the percentage of apoptotic cells increased in the GDH1 depletion group, especially under hypoxia (Fig 1B and C). Supplementation with cell-permeable αKG was successfully executed (Fig EV1C), but the restored αKG did not rescue the effect on HIF1α protein levels (Fig EV1D) and cell viability (Fig EV1E) in the cells lacking GDH1 under hypoxia, indicating that GDH1 might play an intricate role under hypoxia. Measurement of glutamate and ammonia levels reflects the possible conversion of GDH1 enzyme activity under normoxia and hypoxia because the increased glutamate and ammonia concentrations after GDH1 depletion under normoxia were consumed under hypoxia (Fig EV1F and G). Supplementation with octyl-2-hydroxyglutarate (2HG) also had no significant effect on HIF1α protein stability, suggesting that globally increased 2HG does not efficiently compete with αKG for EGLN1 binding (Fig EV1H). Under hypoxia, HIF1α protein levels in the control groups were higher than those in GDH1-depleted cells, while HIF2α protein levels were slightly decreased after GDH1 depletion (Fig 1D). Compared with control cells, HIF1α protein levels were higher in CRC cells overexpressing GDH1, and overexpression of GDH1 conferred CRC cell resistance to hypoxia and resulted in a

lower percentage of apoptotic cells *in vitro* and *in vivo* (Fig EV1I–L). The overall αKG content increased under hypoxia compared with normoxia. Loss of GDH1 impaired the increase in the overall αKG level under normoxia but not hypoxia. Consistent results were observed in cells overexpressing GDH1 under normoxia and hypoxia (Figs 1E and EV1M). These data suggest that GDH1 may not exhibit dehydrogenase activity under hypoxia.

Furthermore, we ruled out the effect of GDH1 on HIF1A transcription levels (Fig 1F), suggesting that GDH1-induced upregulation of the HIF1α protein level is mainly achieved by facilitating the stabilization of HIF1α under hypoxia rather than by affecting the level of gene transcription. The ability of CRC cells lacking GDH1 to form tumors also decreased drastically (Fig 1G and H). To examine GDH1 expression at the clinical level, we assessed the mRNA levels of GDH1 in 16 pairs of CRC and matched paracancerous samples and found that GDH1 did not exhibit high tumor tissue-specific expression (Fig 1I). In tumor tissues, we observed a positive correlation between the GDH1 and HIF1α protein levels (Fig 1J).

Taken together, our primary data suggest that GDH1 participates in regulating HIF1α stability, potentially offering a novel way to stabilize HIF1α.

GDH1 depletion in the mouse intestine impairs CRC progression

To investigate the role of GDH1-mediated oncogenesis *in vivo*, we attempted to construct GDH1 knockout mice but found that mouse embryos showed serious defects and frequently died after GDH1 deletion. Therefore, tissue-specific knockout of GDH1 in the intestine was performed using the Cre-loxP recombination system and was verified by PCR, immunohistochemistry (IHC), and immunoblotting (Figs 2A and B, and EV2A).

The azoxymethane (AOM)/dextran sodium sulfate (DSS) model is a widely used inflammation-associated colon cancer model in rodents (De Robertis *et al*, 2011; Thaker *et al*, 2012). Loss of GDH1 in the intestine significantly reduced the occurrence of CRC in adult mice (Fig 2C). We also observed delayed appearance of tumors after depletion of GDH1 in the mouse intestine (Fig 2D). Furthermore, H&E staining verified the presence of tumors in the intestine (Fig 2E). Of note, equal infiltration of macrophages or microglial cells in the control and GDH1$^{IEC-/-}$ mice was discovered by assessing approximate F4/80 positivity (Fig 2F), and no significant difference was found in the production of proinflammatory cytokines, such as TNFα, IL6, and IFNγ, after AOM/DSS induction in the control and GDH1$^{IEC-/-}$ mice (Fig EV2B). However, focal regions of continuous ZO-1 staining were destroyed in control wild-type mice but remained relatively intact in GDH1-depleted mouse colons (Fig 2G). Mice without GDH1 in the intestine exhibited tolerance to AOM/DSS and a delayed decrease in body weight (Fig 2H). Consistently, GDH1 depletion significantly prolonged the survival time of mice after AOM/DSS treatment (Fig 2I). IHC of GDH1 and HIF1α and H&E staining showed that GDH1 depletion in the intestine limited CRC development and HIF1α levels (Fig 2J). Furthermore, HIF1α protein was almost undetectable in GDH1$^{IEC-/-}$ mice, whereas high levels of HIF1α were found in the intestinal cancer tissues of WT mice treated with AOM/DSS (Fig 2K); however, no significant difference in HIF1A mRNA expression was observed in GDH1$^{IEC-/-}$ and GDH1$^{IEC+/+}$ mice without or with DSS treatment (Fig EV2C). Hence, GDH1 can promote intestinal cancer development, possibly by
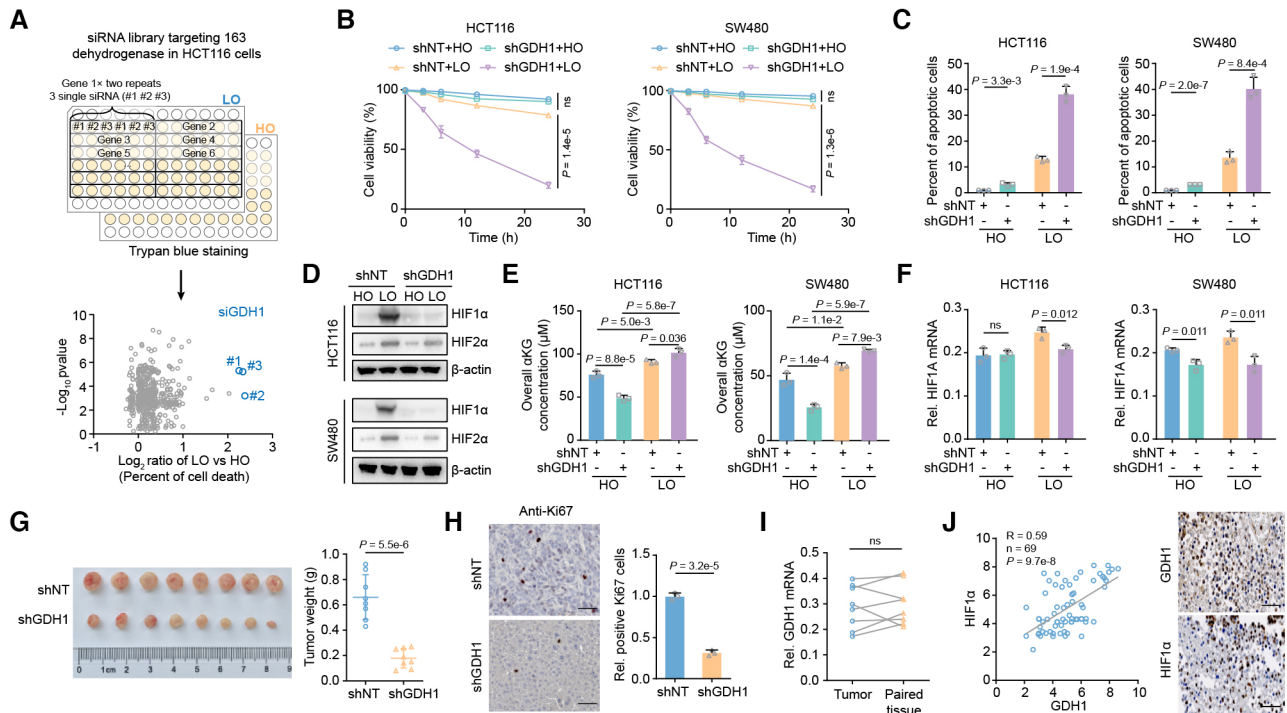
Figure 1. GDH1 confers tumor cell resistance to hypoxia and promotes tumorigenesis.

A   The workflow for screening the dehydrogenase-coding genes required for resisting hypoxia in HCT116 cells. In detail, HCT116 cells were collected and plated in 96-well plates. Cells were transiently transfected with siRNAs separately targeting 163 dehydrogenase-coding genes identified in the KEGG database using RNAiMAX for 36 h, treated with or without hypoxia for 24 h, and finally stained with Trypan blue. The origin of siRNA library was released from horizondiscovery website. The x-axis represents the log$_2$-transformed fold changes in the percentage of dead cells among LO- vs. HO-treated cells. Normoxia, 20% oxygen, is also termed HO. Hypoxia, 0.5% oxygen, is also termed LO.

B   HCT116 and SW480 cells with GDH1 knockdown were incubated under normoxia and hypoxia, respectively. Then, cell viability was assessed by trypan blue staining ($n = 3$).

C   The cells in (B) were collected after incubation under normoxia or hypoxia, and PI/Annexin V double staining was then used to measure the percentage of apoptotic cells via FACS ($n = 3$).

D   The cells in (B) were collected after incubation under normoxia or hypoxia induction for 6 h, and the HIF1α protein level was measured via immunoblot analysis.

E   HCT116 and SW480 cells with GDH1 knockdown were incubated under normoxia and hypoxia, respectively. Then, overall αKG was assessed using an αKG assay kit (Abcam) ($n = 3$).

F   HIF1A gene transcription was slightly impaired after GDH1 depletion. The cells in (B) were collected after incubation under normoxia or hypoxia, and the HIF1A mRNA level was analyzed via quantitative real-time PCR (qRT–PCR) ($n = 3$; ns, not significant).

G, H   Tumor formation study. HCT116-shNT and HCT116-shGDH1 cells were injected into the left groin of nude mice. When the tumor size reached 300 mm^3, the mice were sacrificed, and the tumors were removed for further experiments ($n = 8$) (G). Solid tumors were stained with an antibody against Ki67 (Scale bars: 50 μm) ($n = 3$) (H).

I   The relative mRNA level of GDH1 was determined in 8 paired CRC and adjacent tissues ($n = 8$).

J   Positive correlation between GDH1 and HIF1α protein expression in CRC tissue.

Data information: Data are mean ± SD from the biological replicates (B, C, E–H). Statistics: two-way ANOVA with Tukey's HSD *post hoc* test (B); unpaired two-tailed student's *t*-test (C, F–H, J); one-way ANOVA followed by with Tukey's HSD *post hoc* test (E); paired two-tailed Student's *t*-test (I).
Source data are available online for this figure.

---

increasing HIF1α stability once hypoxia occurs during CRC progression.

Hypoxia-induced acetylation of GDH1 is required for HIF1α stability

To explore the correlation between GDH1 and HIF1α stability, we first excluded the possibility that hypoxia could affect GDH1 protein levels in CRC cells (Fig 3A). Then, we inserted a FLAG tag into the GDH1 C-terminus, which had no effect on GDH1 activity (Fig EV3A and B). Using this system, we enriched GDH1 and observed decreased GDH1 dehydrogenase activity under hypoxia (Fig 3B).

Under hypoxia, the level of GDH1 panlysine (K) acetylation, but not K methylation and S/T/Y phosphorylation, was significantly increased (Fig 3C), suggesting that GDH1 lysine acetylation is involved in the hypoxia response. The enriched GDH1-FLAG was identified by liquid chromatography–mass spectrometry (LC–MS). GDH1 acetylation sites at K503 and K527 were detected under hypoxia but not under normoxia (Fig EV3C and D). Both the mutations of K503 to R503 and K527 to R527 impaired GDH1 acetylation under hypoxia. When these two lysine sites were simultaneously mutated to arginine residues, GDH1 acetylation was heavily impaired (Fig 3D and E). Furthermore, after mutation of K503 and K527 to R503 and R527, respectively, the transcriptional activity of HIF1α
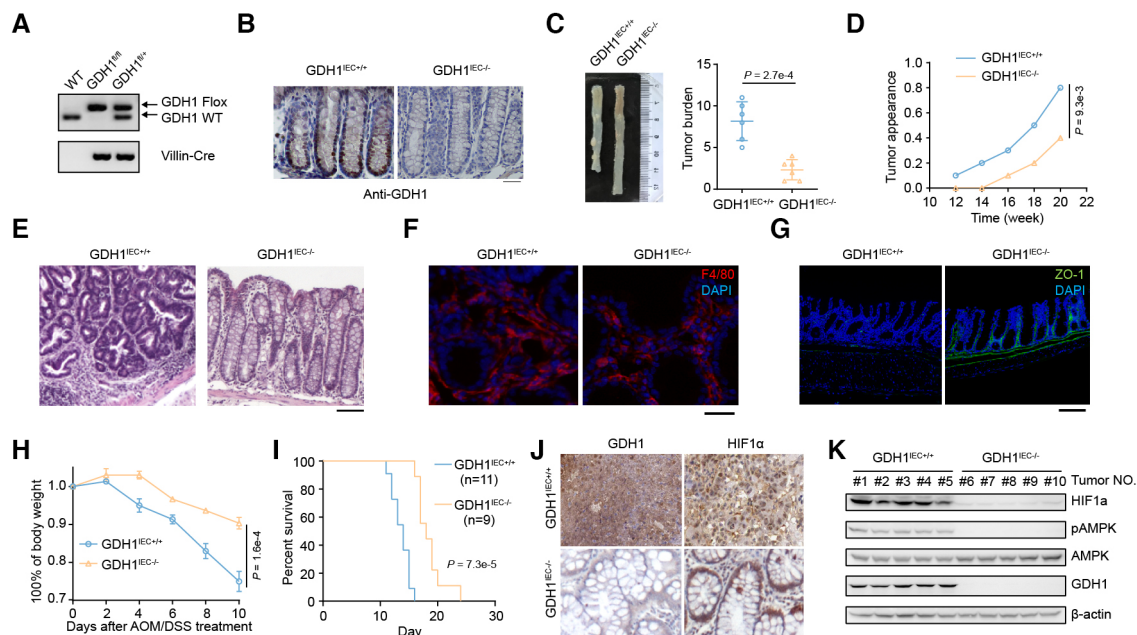
Figure 2. Depletion of GDH1 in the mouse intestine impairs colorectal cancer formation.

A   Identification of GDH1 knockout (KO) in mouse intestines by PCR.

B   Identification of GDH1 KO in mouse intestines by immunohistochemistry (IHC).

C–E   The AOM/DSS-induced inflammatory cancer switch was reduced by the loss of GDH1. (C) Tumor burden ($n = 6$). (D) Tumor appearance. (E) H&E staining of colon cancer tumors from GDH1$^{IEC+/+}$ and GDH1$^{IEC-/-}$ mice (scale bar, 200 μm).

F   F4/80 staining in a noninflamed portion of the colon after AMO/DSS treatment (scale bar, 50 μm).

G   ZO-1 staining in colon sections of mice treated with sequential AMO/DSS treatment (scale bar, 200 μm).

H   Body weight of GDH1$^{IEC+/+}$ and GDH1$^{IEC-/-}$ mice after AOM/DSS treatment ($n = 3$).

I   Survival percentages of GDH1$^{IEC+/+}$ mice ($n = 11$) and GDH1$^{IEC-/-}$ mice ($n = 9$) during progression of the inflammatory cancer switch.

J   GDH1 and HIF1α protein expression in CRC tissue from GDH1$^{IEC+/+}$ mice and GDH1$^{IEC-/-}$ mice.

K   Both HIF1α protein levels and AMPK activity were assessed in the intestine of GDH1$^{IEC-/-}$ mice after AOM/DSS treatment using the indicated antibodies.

Data information: Data are mean ± SD from the biological replicates (C, H). Statistics: unpaired two-tailed Student's t-test (C); two-way ANOVA with Tukey's HSD *post hoc* test (D, H); log-rank test (I).

Source data are available online for this figure.

decreased by approximately 75% (Fig 3F). Meanwhile, the protein levels of HIF1α under hypoxia decreased by more than half after the loss of GDH1 acetylation at K503 or K527 (Fig 3G).

The data showed delayed and weak stabilization of HIF1α protein levels when K503/527 was mutated to R503/527, offering solid evidence that the protein stability of HIF1α is regulated by GDH1 lysine acetylation (Fig 3H and I). Based on these data, we preliminarily ascertained that hypoxia-induced acetylation of GDH1 is required for HIF1α stability.

Hypoxia-induced GDH1 acetylation at K503 reverses GDH1 dehydrogenase activity

How does hypoxia-mediated GDH1 acetylation modulate the protein stability of HIF1α? As shown in Fig 4A and B, GDH1 with the K503R mutation increased the formation of GDH1 hexamers compared with WT GDH1. K527R-GDH1 polymer formation was more or less consistent with that of WT-GDH1 (Fig 4A and B). Hence, we speculated that GDH1 acetylation at K503 regulates GDH1 dehydrogenase activity.

Consistent with this speculation, upon hypoxia stimulation, the relative level of αKG produced by K503R-GDH1 was

significantly increased while The K527R mutation did not affect GDH1 enzyme activity (Fig 4C). However, compared with that of WT-GDH1, the ability of K503R-GDH1 to produce αKG was reduced by around 50%, while the ability of the K503Q-GDH1 mutant to produce glutamate was increased by approximately 130% (Figs EV4A and 4D). In line with the above *in vitro* assay, the relative intracellular αKG content decreased in cells expressing the K503Q mutant, while that in cells expressing the K503R mutant increased under hypoxia compared with that in control cells (Figs EV4B and 4E).

The results of an enzyme kinetics experiment showed that K503Q-GDH1 had a much lower maximum reaction rate (Vmax) of αKG production than GDH1-WT, whereas K503R-GDH1 had a moderately higher Vmax of αKG production than GDH1-WT, suggesting that K503Q-GDH1 has a heavily impaired ability to use glutamate (Glu) as a substrate (Fig 4F). To exclude the possibility that the K to Q mutation does not effectively mimic acetylation modification, we also purified AcK503-GDH1, K503Q-GDH1, and K503R expressed in *E. coli* (Fig EV4C). The qualities and activities of the above proteins were ascertained by a series of *in vitro* experiments, such as LC–MS for modification identification, FPLC and dynamic light scattering
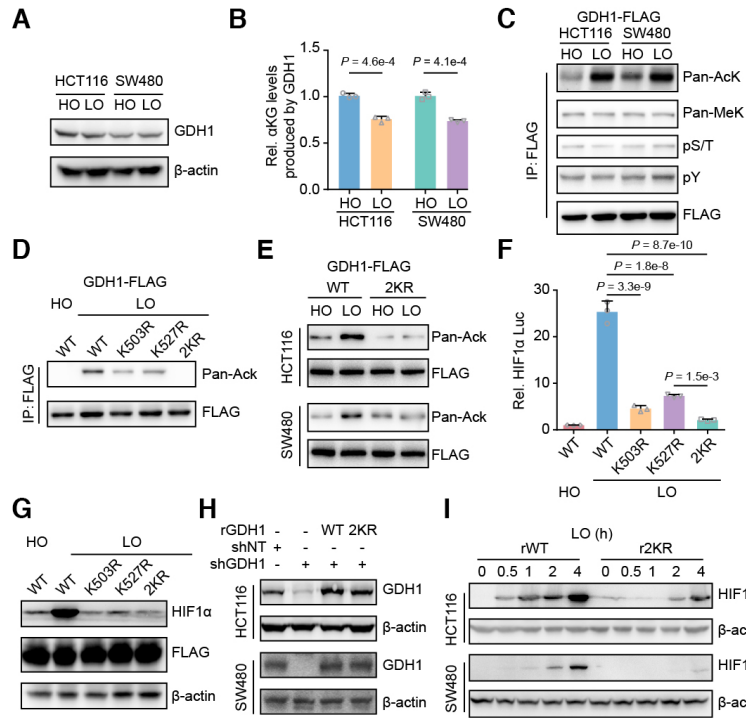
Figure 3. Hypoxia-induced GDH1 acetylation was required for HIF1α stability.

A HCT116 and SW480 cells were incubated under normoxia and hypoxia, respectively. Then, the cells were collected, and the GDH1 protein level was analyzed via immunoblotting.

B Hypoxia reduced the activity of GDH1 in producing αKG. A FLAG tag was inserted into the GDH1 C-terminus in HCT116 and SW480 cells. The cells were collected after incubation under normoxia or hypoxia, and M2 flag beads were used to enrich FLAG-tagged GDH1. GDH1-FLAG was used to assess the enzymatic activity of GDH1 in producing αKG ($n = 3$).

C GDH1-FLAG in (B) was examined using antibodies against pan-lysine acetylation and methylation and pan-serine/threonine and tyrosine phosphorylation.

D GDH1 acetylated at both K503 and K527 under hypoxia. K503R and K527R were mutated endogenously. GDH1-FLAG was enriched, and an antibody against pan-lysine acetylation was used to examine lysine acetylation of GDH1 when K503 or K527 was mutated to R503 or R527. 2KR represents K503/K527R.

E HCT116 or SW480 cells containing WT or GDH1 with K503/K527R mutations were incubated under normoxia and hypoxia, respectively. GDH1-FLAG was enriched, and an antibody against pan-lysine acetylation was used to test GDH1-lysine acetylation.

F Loss of acetylation at GDH1-K503 or GDH1-K527 impaired the transcriptional activity of HIF1α ($n = 3$).

G HIF1α protein stability under hypoxia depends on GDH1-K503 and GDH1-K527 acetylation.

H GDH1-depleted cell lines were constructed and then rescued with the expression of wild-type GDH1 or K503/K527R mutant GDH1.

I HIF1α protein stability in rWT or r2KR mutant cells was induced over time under hypoxia.

Data information: Data are mean ± SD from the biological replicates (B, F). Statistics: unpaired two-tailed Student's *t*-test (B); one-way ANOVA with Tukey's HSD *post hoc* test (F).

Source data are available online for this figure.

(DLC) to determine dimerization and NADH measurement to assess GDH1 dehydrogenase activity (Fig EV4D–G). AcK503-GDH1 had a Vmax of αKG or Glu production similar to that of K503Q-GDH1, demonstrating that the K503Q mutant mimics acetylation at K503 (Fig 4G). Moreover, we experimentally defined the Michaelis–Menten constant (*Km*) value of these GDH1 variants for Glu. The calculated *Km* value indicated that K503Q-GDH1 had a much lower Glu affinity than GDH1-WT, whereas K503R-GDH1 had a higher Glu affinity than GDH1-WT (Fig 4H). Isothermal titration calorimetry (ITC) further showed that AcK503- and K503Q-GDH1 showed increased GDH1 to αKG binding affinity compared with WT or K503R-GDH1, which was consistent with the results of previous enzyme assays in which the K503Q mutation reduced the ability of GDH1 to produce αKG (Fig 4I). We also summarized the effect of K503 acetylation on the exchange of the GDH1 trimer and hexamer, which indicates the conversion of GDH1 activity (Fig 4J).

Notably, the K503Q mutation reduced the binding affinity of Glu to GDH1 but had no effect on NAD$^+$ binding to GDH1 (Fig EV4H and I). Molecular simulation revealed that GDH1-His (H) 266, -H507 and GTP form a hydrogen bond network and that hypoxia-induced acetylation at K503 of GDH1 locks GTP in the hydrogen bond network of H266-H507, in turn reinforcing αKG in GDH1 as a substrate. Otherwise, the position of K527 is located in a large flat groove and facilitates GDH1 association with other partner proteins (Fig EV4J). Thus, we preliminarily conclude that under hypoxia, GDH1 enzyme activity is reversed by acetylation at K503.

Hypoxia-induced GDH1 acetylation at K527 anchors GDH1 to the EGLN1/HIF1α complex

To find the correlation between HIF1α stability and the overall αKG content, we overexpressed certain enzymes that produce or
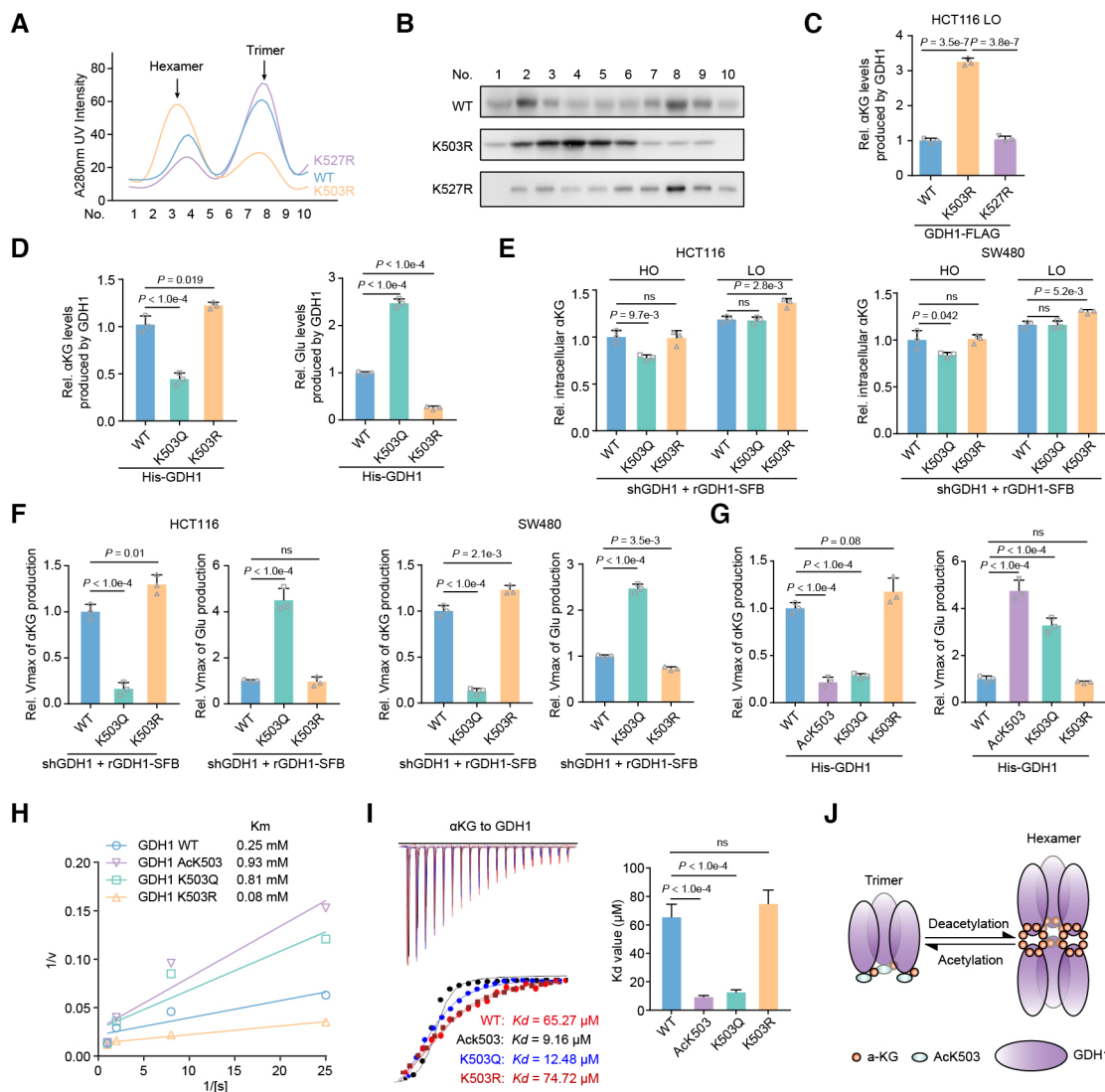
Figure 4. GDH1 acetylation at K503 reverses GDH1 dehydrogenase activity through decreased formation of GDH1 hexamers.

A   GDH1-FLAG (including WT and K503R and K527R mutants) was enriched and analyzed via fast protein liquid chromatography (FPLC).

B   Immunoblot analysis of GDH1-FLAG levels at different time points.

C   The K503R mutation enhances GDH1 activity in producing αKG. FLAG-tagged GDH1 was purified from HCT116 cells (*n* = 3).

D   The K503Q mutation reduces GDH1 activity leading to αKG production while enhancing the enzymatic activity leading to Glu production. His-tagged GDH1 was purified from *E. coli* (*n* = 3).

E, F   HCT116 or SW480 cells were depleted of endogenous GDH1 and rescued with SFB-tagged rGDH1 WT, K503Q or K503R. The relative intracellular αKG concentration was measured under normoxia and hypoxia (E). rGDH1-SFB proteins were enriched using M2-FLAG beads to determine the Vmax of αKG production (F) (*n* = 3).

G–I   His-GDH1 proteins (including WT, AcK503, K503Q and K503R) were purified from *E. coli* to determine the Vmax of αKG and Glu production (G). A Lineweaver–Burk plot was used to determine the Michaelis–Menten constant (*Km*) value for Glu production by the GDH1 proteins (H). V, reaction rate; [S], substrate concentration. ITC assays were performed with precipitated His-GDH1 proteins and αKG (I) (*n* = 3).

J   Cartoon illustrating the working mechanism of the GDH1 acetylation-mediated decrease in hexamers and the enhanced binding affinity to αKG.

Data information: Data are mean ± SD from the biological replicates (C–G, I). Statistics: one-way ANOVA with Tukey's HSD *post hoc* test (C–G, I).
Source data are available online for this figure.

consume αKG, and we observed that HIF1α protein was not regulated by global changes in αKG (Fig 5A and B). Furthermore, to elucidate the mechanism by which GDH1 mediates HIF1α protein stability, we applied liquid chromatography coupled with tandem mass spectrometry (LC–MS/MS) to verify both HIF1α and EGLN1 as GDH1-interacting proteins under hypoxia (Fig 5C). Reverse Co-IP

was performed to test whether EGLN1 interacts with other αKG producers or consumers, such as BCAT1/2, GOT1/2, IDH1/2, and GPT (Fig EV5A). Using fraction assays and immunofluorescence (IF) experiments, we clarified that GDH1 interacts and colocalizes with EGLN1 in the cytosol upon hypoxia (Fig 5D and E). Under hypoxia, GDH1 accumulated in the cytosol but showed a slightly decreased

Figure 5.

Figure 5. Tumor cells require both GDH1-K503 and GDH1-K527 acetylation to simultaneously reduce EGLN1 activity under hypoxia.

A, B   Immunoblot of the HIF1α protein level under hypoxia for 6 h when enzymes related to the αKG level were overexpressed in cells, including GDH1 (A). Relative αKG levels in contrast to the control (B) ($n = 3$).

C   HCT116-GDH1-FLAG cells were incubated under normoxia and hypoxia. Cells were then collected, and M2 flag beads were used to enrich FLAG-tagged GDH1. GDH1-FLAG-associated proteins were identified by LC–MS/MS. The fold change was evaluated as the ratio of expression under hypoxia to that under normoxia. The x-axis represents the $\log_2$-transformed fold change, and the y-axis represents the minus $\log_{10}$-transformed P-value.

D   A Co-IP assay was performed to test the interaction between GDH1 and EGLN1 in the cytosolic and mitochondrial fractions from HCT116-GDH1-FLAG cells.

E   Immunofluorescence analysis of GDH1-FLAG and HA-EGLN1 was performed to assess their colocalization under normoxia and hypoxia.

F   GDH1-FLAG was enriched in the cytosolic and mitochondrial fractions from HCT116-GDH1-FLAG cells, and the enzymatic activity of GDH1 in producing αKG was evaluated ($n = 3$).

G   HCT116 cells were cotransfected with plasmids encoding GDH1-FLAG and HA-EGLN1. A Co-IP assay was performed to examine whether the K503R or K527R mutation affected the interaction between GDH1 and EGLN1.

H, I   EGLN1 activity test. After hypoxia stimulation for 1 h, HA-EGLN1 was enriched in HCT116-shGDH1 cells restored with WT or mutant GDH1 (H). His-GDH1 with K503 or K527 acetylation (AcK503 or AcK527) and mimic acetylation at K503 or K527 (K503Q or K527Q) were purified from *E. coli*. Then, His-GDH1 was incubated for 1 h with HA-EGLN1 (I). EGLN1 activity was tested by converting αKG to succinate ($n = 3$).

J, K   Relative αKG content in EGLN1. HA-EGLN1 was enriched in shNT or shGDH1 cells under hypoxia. A radiometric ^{14}C-αKG-EGLN1 binding assay was performed using HA-EGLN1 incubated with ^{14}C-αKG (J). Alternatively, the HA-EGLN1 protein was digested by trypsin, and αKG was determined by LC–MS/MS analysis (K) ($n = 3$).

L–N   Detection of HIF1α protein stability (L); the mRNA expression levels of the HIF1α target genes GLUT1, HK1, PGK1 and CCND1 (M); and HIF1α transactivation (N) in the indicated cell lines under hypoxia ($n = 3$).

O   Detection of HIF1α protein stability in the indicated cell lines under normoxia.

P   HIF1α transactivation was examined in the indicated cell lines under hypoxia with or without treatment with the HIF1α transactivation inhibitor 2-MeOE2 (1 μM) for 12 h ($n = 3$).

Data information: Data are mean ± SD from the biological replicates (B, F, H–K, M, N, P). Statistics: one-way ANOVA with Tukey's HSD *post hoc* test (B, F, H–K, M, N, P); unpaired two-tailed Student's *t*-test (C).
Source data are available online for this figure.

presence in mitochondria. More importantly, cytosolic GDH1 presented lower dehydrogenase activity (Fig 5F). Furthermore, we performed a Co-IP assay and found that loss of GDH1 acetylation at K527 abolished the interaction between GDH1 and EGLN1 (Fig 5G). Mimicked acetylation at K503 or K527 reduced EGLN1 hydroxylase activity, while the loss of acetylation at K503 or K527 dramatically enhanced EGLN1 hydroxylase activity even under hypoxia (Fig 5H). We purified GDH1 with lysine acetylation or with mimicked acetylation expressed in *E. coli* or HCT116 cells, respectively, and then tested whether antibodies specifically targeted the corresponding lysine acetylation (Fig EV5B). By incubating the above purified GDH1 proteins with EGLN1, we found that GDH1 acetylation at K503 but not at K527 constrained EGLN1 hydroxylase activity (Fig 5I). A potential explanation for this result is that GDH1 combined with EGLN1 in this *in vitro* reaction system and the effect of K527 acetylation was not reflected. As hypoxia drives GDH1 acetylation and targets EGLN1, the overexpression of WT-GDH1 dramatically impaired EGLN1 activity upon hypoxia (Fig EV5C).

To test whether EGLN1-bound αKG is regulated by GDH1 acetylation at K503 or K527, we developed a radiometric ^{14}C-αKG-EGLN1 binding assay and LC–MS-based protein-bound metabolite assay. The consistent results of these two assays confirmed that acetylation at the K503 and K527 sites is indispensable for reducing the possibility of αKG binding to EGLN1 under hypoxia (Fig 5J and K). The specificity of the above assays to measure EGLN1-bound αKG was confirmed using an EGLN1 R383/398A mutant, which lost the ability to capture αKG, and we observed a competitive effect of WT-GDH1 overexpression on EGLN1-bound αKG (Fig EV5D and E). Otherwise, EGLN1 activity was reduced in K503Q-GDH1 cells (Fig EV5F). The acetylation of GDH1 at K503 or K527 is essential for maintenance of the stability of HIF1α under hypoxia. In detail, the individual K503R and K527R mutations resulted in HIF1α instability, and the 2KR double mutation reinforced this effect (Fig 5L). The expression of the HIF1α downstream genes GLUT1, HK1, PGK1, and

CCND1 (Semenza, 2003; Luo *et al*, 2006) was also significantly reduced when GDH1 deacetylation occurred or was mimicked (Figs 5M and EV5G). In line with this, HIF1α transactivation was impaired by deacetylation at K503 or K527, and this impairment was reinforced by the 2KR mutant in GDH1 (Fig 5N). Simultaneously, mutating K503 and K527 to mimic constitutive acetylation significantly enhanced the stability of HIF1α under normoxia (Fig 5O). The increased HIF1α stability induced by GDH1 acetylation at K503 and K527 was abolished by the HIF1α transactivation inhibitor 2-MeOE2 (Fig 5P).

We also assessed the effect of individual mimic acetylation mutations on HIF1α and found that mimic acetylation at K503 or K527 alone did not have a sufficient capacity to stabilize HIF1α under hypoxia (Fig EV5H) by exhausting αKG in EGLN1 (Fig EV5I and J) and impaired EGLN1 activity (Fig EV5K and L). Finally, the individual mimic acetylation mutations in GDH1 did not drive gene expression mediated by HIF1α (Fig EV5M).

Hence, upon hypoxia exposure, GDH1-K527 acetylation targets EGLN1, while GDH1-K503 acetylation produces glutamate using αKG as a substrate. The conversion of GDH1 enzyme activity prompts HIF1α stability by consuming αKG in the GDH1/EGLN1/HIF1α axis.

p300 acetylates GDH1 in cytosol

Using the K503R-GDH1 or K527R-GDH1 mutant to exclude nonspecific recognition, both antibodies were found to specifically identify GDH1 acetylation under hypoxia (Fig 6A) and indicated that the extent of AcK503 and AcK527 increased with prolonged hypoxia treatment time (Fig 6B). GDH1-AcK503 and GDH1-AcK527 were present in both the cytosol and nucleus (Fig 6C).

TIP60, PCAF, CBP, and p300 are four major acetyltransferases responsible for lysine acetylation (Wapenaar & Dekker, 2016). The knockdown efficiency of small interfering RNAs specifically
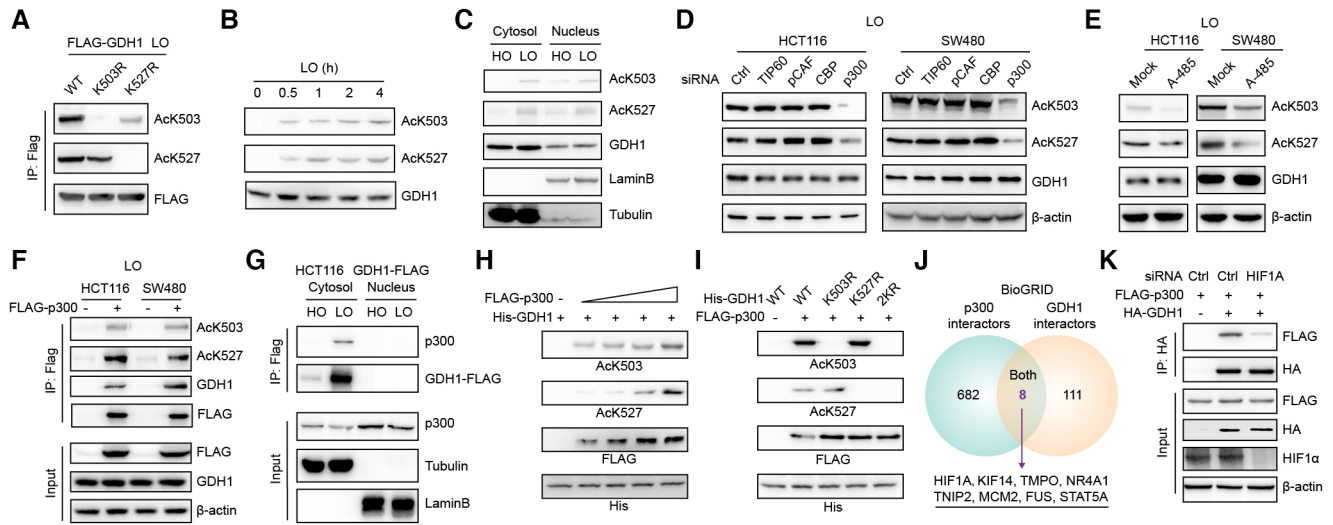
Figure 6. p300 acetylates GDH1 at K503 and K527 under hypoxia.

A   Immunoblot analysis identified the specificity of the antibody against GDH1-K503 or GDH1-K527 acetylation.

B   GDH1-K503 or GDH1-K527 acetylation increased with the time course of hypoxic stress.

C   GDH1-K503 or GDH1-K527 acetylation occurred in both the cytosol and nucleus.

D, E The levels of both AcK503 and AcK527 were analyzed when cells were transfected with small interfering RNA (siRNA) targeting TIP60, PCAF, CBP or p300 (D) or when HCT116 or SW480 cells were treated with the p300 inhibitor A-485 (1 μM) for 12 h under hypoxia (E).

F   HCT116 and SW480 cells were transfected with or without FLAG-p300. The p300-associated proteins were enriched with M2-FLAG beads and subjected to immuno-blot analysis using antibodies against GDH1, GDH1-K503 or GDH1-K527 acetylation.

G   A Co-IP assay was performed to examine the interaction between GDH1 and p300 in the cytosolic and nuclear fractions of HCT116 GDH1-FLAG cells.

H   p300 acetylated GDH1 at K503 and K527 in a dose-dependent manner.

I   p300 specifically acetylates GDH1 at K503 and K527.

J   The GDH1 and p300 interacting proteins were extracted from the BioGrid database, and the shared interacting proteins are shown in a Venn diagram.

K   The HIF1A gene was transiently knocked down, and HCT116 cells were cotransfected with FLAG-p300 and HA-GDH1 for a Co-IP assay.

Source data are available online for this figure.

targeting the genes encoding the above acetyltransferases is shown in Appendix Fig S1A. p300 depletion induced a decrease in AcK503 and AcK527, while the knockdown of the other acetyltransferases did not have this effect (Fig 6D). Furthermore, using an inhibitor specifically targeting p300, we observed a result consistent with that obtained by p300 depletion with specific siRNA (Fig 6E). Co-IP experiments showed that the FLAG-p300-associated complex contained GDH1 acetylated at K503 and K527 (Fig 6F). Co-IP analyses of cytosolic and nuclear fractions identified GDH1 and p300 interacting in the cytosol but not in nuclei, suggesting that nuclear AcK503-GDH1 and AcK527-GDH1 first occurred in the cytoplasm (Fig 6G). As shown in the BioGRID database, approximately 30% of p300 interactors are localized in the cytosol (Appendix Fig S1B), and IF staining using an antibody against p300 showed that p300 localized in both the cytosol and nucleus (Appendix Fig S1C). Moreover, the HIF1α protein level was blocked by p300 knockdown in WT-GDH1-overexpressing cells but not in 2KQ-GDH1-overexpressing cells (Appendix Fig S1D). These results demonstrate that p300 is required for GDH1 acetylation.

We also performed a semi-*in vitro* biochemical experiment in which gradually increased FLAG-p300 purified from HCT116 cells was incubated with His-GDH1 purified from *E. coli*, and the levels of AcK503-GDH1 and AcK527-GDH1 increased in this *in vitro* acetylation reaction system (Fig 6H). When we mutated K503 to R503 or K527 to R527, no signals for GDH1 acetylated at K503 or K527 were

detected, even when p300 was added to the acetylation reaction system (Fig 6I). To clarify how GDH1 recruits p300, we evaluated the common interacting proteins of GDH1 and p300 in the BioGrid database. As shown in Fig 6J, eight proteins, including HIF1α, were potential bridges linking p300 to GDH1. We first transiently knocked down the HIF1A gene and found that HIF1A depletion resulted in an obvious reduction in the interaction between GDH1 and p300 (Fig 6K). The above results further confirm that p300 forms an axis with GDH1/HIF1α and is responsible for acetylating GDH1 at K503 and K527.

GDH1 acetylation at both K503 and K527 is required to form solid tumors and is correlated with a poor CRC prognosis

Under hypoxia, the expression of the individual GDH1 K503R or GDH1 K527R mutant sensitized cells to hypoxia, and the GDH1 2KR mutant reinforced this effect (Fig 7A and Appendix Fig S2A). Consistently, only approximately 7% of 2KQ-GDH1 mutant cells were apoptotic. Under the same conditions, more than 30% of K503R-, K527R- or 2KR-GDH1 mutant cells were apoptotic (Fig 7B, Appendix Fig S2B and C). Moreover, HIF1α knockdown blocked the increased resistance to apoptosis of WT or 2KQ-GDH1 cells under hypoxia but not of GDH1 knockdown cells, further supporting the existence of the GDH1/EGLN1/HIF1α axis (Appendix Fig S2D). Experiments in tumor-bearing nude mice showed that GDH1 acetylation was
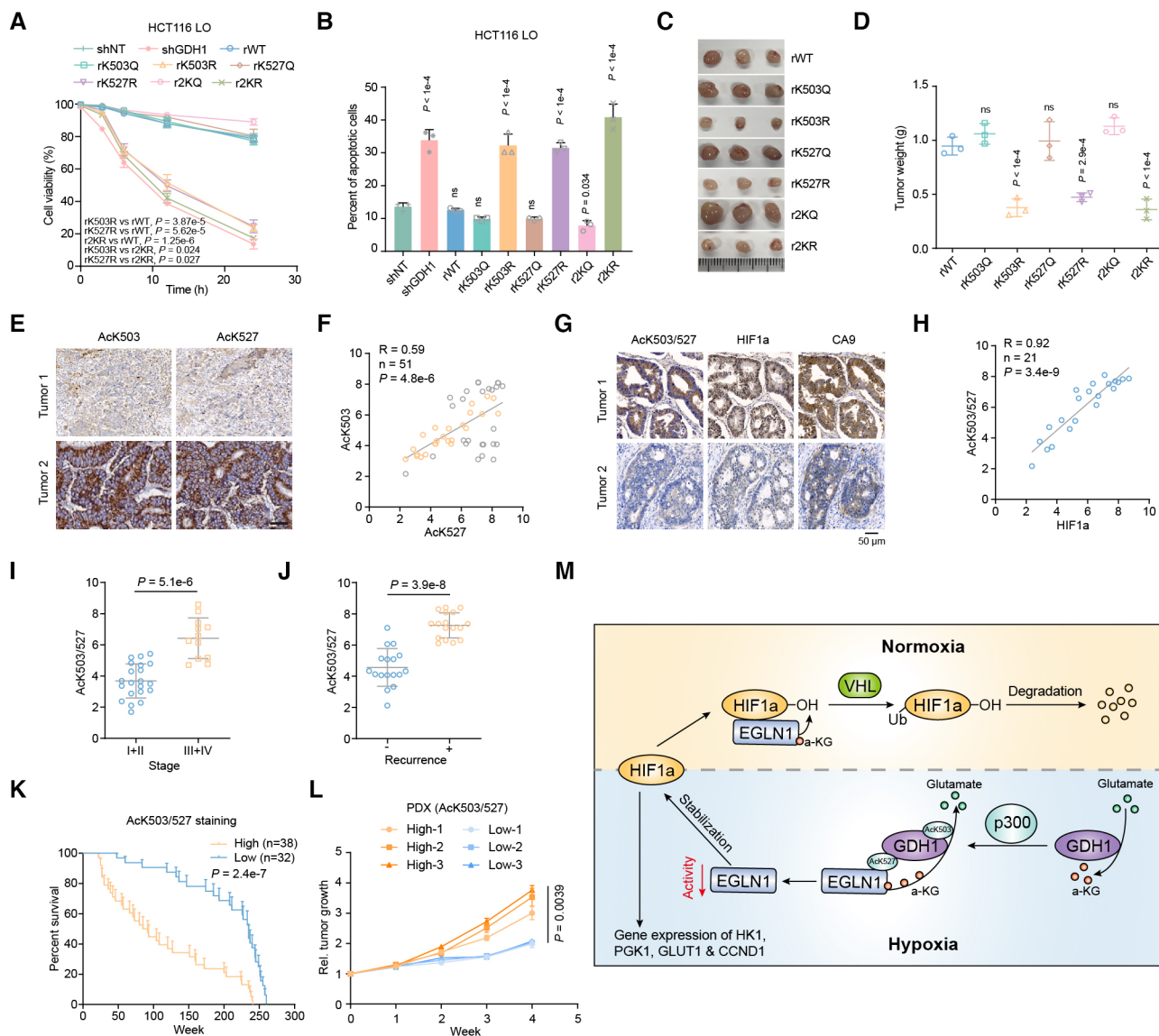
Figure 7. AcK503/527-GDH1 indicates a poor prognosis, mainly dependent on HIF1α stabilization.

A, B   Cell viability and percentage of apoptosis in the indicated cell lines under hypoxia were analyzed by trypan blue (A) and PI/Annexin V double staining (B), respectively (*n* = 3).

C, D   The xenograft tumor formation efficiency of the indicated cell lines was assessed, and tumor weight measurements were performed (*n* = 3).

E   Representative images of CRC samples are shown after antibody staining of AcK503-GDH1 and AcK527-GDH1.

F   The correlation between AcK503-GDH1 and AcK527-GDH1 expression in CRC samples. The tissue sections were quantitatively scored according to the percentage of positive cells and the staining intensity (*H*-score) (*n* = 51).

G   Representative images of the same CRC samples are shown after staining with antibodies against AcK503/527-GDH1 and HIF1α.

H   Correlation between AcK503/527-GDH1 and HIF1α expression in CRC samples (*n* = 21).

I   Detection of AcK503/527-GDH1 expression in CRC grades I + II and III + IV (grade I + II, *n* = 21; grade III + IV, *n* = 12).

J   Detection of AcK503/527-GDH1 expression in patients with (+) or without (−) recurrence (−, *n* = 17; +, *n* = 17).

K   Patient survival corresponding to different levels of AcK503/527-GDH1 expression (High, *n* = 38; Low, *n* = 32).

L   PDX growth related to high or low levels of AcK503/527-GDH1 expression.

M   Schematic model described in the discussion section.

Data information: Data are mean ± SD from the biological replicates (A, B, D, I, J, L). Statistics: two-way ANOVA with Tukey's HSD *post hoc* test (A, L); one-way ANOVA with Tukey's HSD *post hoc* test (B, D); unpaired two-tailed Student's *t*-test (F, H); Mann–Whitney *U*-test (I, J); log-rank test (K). Source data are available online for this figure.

required for the formation of solid tumors. A lack of GDH1 acetylation at K503 or K527 significantly decreased the ability of cells to form solid tumors (Fig 7C and D).

Because the simultaneous acetylation of GDH1 at K503 and K527 is required to maintain HIF1α stability, we first examined the correlation between AcK503 and AcK527 and then selected samples in

which AcK503 and AcK527 were highly positively correlated for subsequent experiments (Appendix Fig S2E, Fig 7E and F). To investigate the correlation between AcK503/527-GDH1 and HIF1α at the tissue level, we prepared an antibody against AcK503/527-GDH1 by mixing the two acetylated peptides (Appendix Fig S2F–H). The AcK503/527-GDH1 and HIF1α signals in tissues were highly positively correlated, indicating that HIF1α protein stability is upregulated when GDH1 is diacetylated at K503/527 in the clinic (Fig 7G and H). The tumor tissue from AOM/DSS mice also presented a similar correlation between AcK503/527-GDH1 and HIF1α in hypoxic regions (Appendix Fig S2I). The above experiments revealed that AcK503-GDH1/K527 is positively correlated with the degree of CRC malignancy (Fig 7I and J) and is expected to be a biomarker to characterize CRC progression and prognosis. Furthermore, we calculated the survival duration of patients in the two groups depending on their level of acetylated K503/K527-GDH1. Patients with high AcK503/527-GDH1 expression clearly presented a shorter survival time than those with low expression (Fig 7K). We observed a higher tumor growth rate in patient-derived xenografts (PDXs) from patients with a high AcK503/527-GDH1 expression (Fig 7L). The above data suggest that GDH1 acetylation at K503/K527 can indicate CRC progression under hypoxia.

Discussion

In this study, through siRNA screening targeting 163 dehydrogenase-coding genes, we found that GDH1 could confer tolerance to hypoxia. The effects of metabolic enzyme defects on organ development and pathology have been poorly studied. Using the Cre-loxP recombination system to selectively deplete metabolic enzymes in specific organs, we obtained a mouse model lacking the GDH1 gene in the small intestine. Although GDH1 knockout had no significant effect on intestinal development, AOM/DSS treatment did not effectively induce CRC in mice with GDH1 deletion in the intestine. Hence, first, through a series of in vitro and in vivo experiments, we ascertained the oncogenic role of GDH1 in CRC development by adapting tumor cells to hypoxic stress.

The formation of blood vessels occurs later in the process of solid tumor formation, which subjects solid tumors to many stresses, such as hypoxia and nutrient limitation (Hanahan & Weinberg, 2011). Solid tumors have developed strategies to address these stresses and survive. Here, we examined the stress response signaling pathways associated with hypoxia and nutrient limitation. AMPK phosphorylation and HIF1α levels were significantly lower in CRC tissues of GDH1-deficient mice than in those of WT mice. We previously reported that GDH1 regulates AMPK phosphorylation under glucose deficiency (Wang et al, 2019a). In the present study, we found that GDH1 also plays a role in modulating HIF1α stability. HIF1α regulates a wide range of target genes involved in tumor cell growth, such as GLUT1, HK1, PGK1, and CCND1 (Semenza, 2003). Consequently, the expression of these genes was significantly decreased in GDH1-deficient CRC cells.

In both cell lines and animal models, we preliminarily verified that GDH1 is required to stabilize HIF1α under hypoxia. In different cellular contexts, GDH1 depletion results in a 25–60% decrease in intracellular αKG levels (Yang et al, 2009; Jin et al, 2015). Given that αKG is a cofactor for members of the TET, DNMT, and EGLN

families, it is reasonable to hypothesize that changes in the level of αKG would alter the activity of these enzymes. EGLN family depends on multiple substrates and cofactors for activity, including αKG, 2HG, and iron availability, and on the presence of oxidative stress (Ke & Costa, 2006; Kaelin & Ratcliffe, 2008). It is reported that EGLN1 activity is not only regulated by oxygen but also regulated by the intracellular metabolite αKG, which competes with its analogue 2HG. For example, BCAT1 is reported to restrict αKG levels and thus promote glioma occurrence and survival by decreasing EGLN1 enzyme activity and increasing HIF1α protein stability (Raffel et al, 2017); therefore, a correlation between BCAT1 and EGLN1 can be proposed. However, biochemistry indicators were not examined in their study. In fact, the Km value of EGLN1 for αKG is 1.3 μM (Lorenzo et al, 2014), while in different cell contexts, the intracellular αKG concentration changed in the range of 10–200 μM, which was insufficient to affect EGLN1 enzyme activity. Meanwhile, although 2HG is a well-established competitive inhibitor of αKG, the global increase in 2HG induced by supplementation with cell-permeable octyl-2HG had no effects on EGLN1 activity in this study. This result was supported by a previous report showing that the IDH1-R132H mutant utilized αKG as a substrate and produced R-2HG, which did not stabilize HIF1α protein (Koivunen et al, 2012). Conversely, forced expression of an IDH1-R132H mutant reduced αKG but increases HIF1α protein (Zhao et al, 2009). The inconsistent results of the above studies suggest that global changes in intracellular αKG or 2HG do not uniformly affect EGLN1 activity. Thus, we should shift our perspective toward signal transduction-mediated local changes in αKG.

Under hypoxia, GDH1 undergoes simultaneous acetylation at K503 and K527, which regulate GDH1 enzyme activity and target the EGLN1/HIF1α complex, respectively. Lysine acetylation modifies enzyme activity, protein stability, and protein–protein interactions, among other effects (Choudhary et al, 2014). Hypoxia-induced GDH1 acetylation at K503 likely confers resistance to αKG feedback inhibition of GDH1, after which GDH1 can use αKG as a substrate to produce glutamate. The direction of the reaction will be determined when the concentrations of the substrate and product are no longer changed by the enzyme. A reversible reaction would occur if the accumulation of the product or the affinity of the enzyme to the product exhibits a significant increase. We previously reported that PGK1 phosphorylation caused a reversible reaction upon the stimulation of resident tissue macrophages secreting IL-6 (Zhang et al, 2018).

To ascertain the effect of the hypoxia-induced interaction between GDH1 and EGLN1 and of the decreased GDH1 αKG production activity on EGLN1 activity, we performed a series of experiments, as shown in Fig 5F–L. We first determined EGLN1 activity in cells with different genetic manipulations and used an in vitro assay in which different GDH1 mutants were incubated with EGLN1, and the results preliminarily linked GDH1 K503 and K527 acetylation to EGLN1 activity. Next, we applied both a radiometric ^{14}C-αKG-EGLN1 binding assay and IP-LC/MS determination to identify the relative quantity of EGLN1 binding to αKG. Taken together, the data showed that a reverse GDH1 enzyme reaction occurred upon hypoxia and exhausted αKG around EGLN1 or impaired the affinity of EGLN1 for αKG.

p300 has been reported to positively regulate HIF1α protein stability (Geng et al, 2012), and MUC1 has been shown to physically interact with HIF1α and p300 to stabilize HIF1α at the protein level

(Chaika *et al*, 2012). Consistently, we confirmed that p300 acetylated GDH1 under hypoxia and linked p300 to EGLN1 activity and HIF1α stability. Moreover, HIF1α significantly promoted the interaction between GDH1 and p300, and upregulated GDH1 acetylation. The initiation of GDH1 acetylation primarily promoted HIF1α stabilization, which in turn promoted the interaction between GDH1 and p300, forming a positive cycle for fast accumulation of HIF1α and a rapid response to hypoxic stress. This should be an important positive feedback loop which allows tumor cells to survive when facing hypoxia.

Although metabolic reprogramming is a hallmark of tumorigenesis and progression, little is known about the metabolic enzymes and oncometabolites that regulate CRC resistance to hypoxia and facilitate survival, and very few metabolic enzymes or molecules have been identified as potential biomarkers *in situ* (Sullivan *et al*, 2016). In this study, GDH1 acetylation at K527 facilitated GDH1 anchoring of EGLN1/HIF1α, while GDH1 acetylation at K503 drove GDH1 to use αKG as a substrate to produce glutamate, the progression of which reduced the concentration of αKG around/in the EGLN1/HIF1α complex or impaired the capacity of EGLN1 to bind αKG, both of which in turn stabilized HIF1α. Therefore, the hypoxia-modulated acetylation of GDH1 at K503 and K527 is a potential biomarker of CRC progression, and the GDH1/EGLN1 axis is a potential target for CRC treatment (Fig 7M).

Materials and Methods

Patient specimens

Tumors and adjacent colorectal tissues were obtained from patients with CRC who underwent surgery or biopsy at The First Affiliated Hospital and The Third Affiliated Hospital of Sun Yat-sen University between 2012/08 and 2017/03. The patients had not received any chemotherapies or other treatments before surgery treatment or diagnosis at the hospital, harboring high or low AJCC stage level. The clinicopathological information was supplied in Tables EV1–EV4. The study protocol was approved by the Ethics Committee of Sun Yat-sen University (Guangzhou, China, ethics approval: #fahsysu-038). Written informed consent was obtained from all participants in this study. All the research was carried out in accordance with the provisions of the Declaration of Helsinki of 1975 and the Department of Health and Human Services Belmont Report.

IHC analysis

Tissue sections from paraffin-embedded human CRC tissues were stained with antibodies as indicated. We quantitatively scored the tissue sections according to the percentage of positive cells and the staining intensity. We rated the intensity of staining on a scale of 0–3: 0, negative; 1, weak; 2, moderate; and 3, strong. We assigned the following proportion scores: X indicates the percentage of the tumor cells that were stained $(0 \leq [X1 + X2 + X3] \leq 10)$, where X3 indicates strong staining, X2 moderate staining and X1 weak staining. The score (*H*-score) was obtained using the following formula: $3 \times X1 + 2 \times X2 + 1 \times X3$, yielding scores ranging from 0 to 10. Scores were compared with overall survival, defined as the time from the date of diagnosis to death or the last known date of follow-up. The use of

human CRC specimens was approved by the IRB at Sun Yat-sen University Guangzhou Cancer Center and complied with all relevant ethical regulations. Informed consent was obtained from all patients.

AOM/DSS-induced colitis-associated colon cancer model

All mice were maintained under a 12-h light/dark cycle with free access to water and standard mouse chow in a specific-pathogen-free (SPF) facility, receiving humane care. All experimental procedures were performed in compliance with the Guide for the Care and Use of Laboratory Animals and approved by the Institutional Animal Care and Use Committee (IACUC) in Guangzhou University (Guangzhou, China, ethics approval: #gzhu2018039).

In the present study, the effect of AOM injection and DSS dietary administration was evaluated in GDH1$^{IEC-/-}$ mice and control wild-type mice in C57BL/6 background. On Day 0, mice were given a single intraperitoneal injection of AOM (10 mg/kg body weight) at the age of 7 weeks old. Seven days after the AOM injection, the animals received 2% DSS (w/v) in the drinking water for 7 days, and then, drinking water alone was supplied for 7 days. The DSS-to-water cycle was repeated a total of three times. All animals were sacrificed on Day 80. At the time of sacrifice, a complete necropsy was performed on all mice. Histopathological examination was performed on paraffin-embedded sections after hematoxylin and eosin (H&E) staining.

Plasmids

pCDH-GDH1 and pColdI-His-GDH1 were constructed in a previous study (Wang *et al*, 2019a), as was pCDH-p300 (Wang *et al*, 2017). PCR-amplified HIF1α was cloned into pCDH-GDH1. K503R/Q and K527R/Q mutations were generated using a QuickChange site-directed mutagenesis kit (Stratagene, La Jolla, CA, USA).

The pGIPZ control and pGIPZ GDH1 shRNA were generated as previously described (Wang *et al*, 2019a). The HIF1α reporter plasmid was generated using the sequences cloned into the pGL3-TA promoter, and the sequence is listed in a previous report (Wang *et al*, 2019a).

Cell culture, transfection and designed antibody

Human CRC HCT116 and SW480 cell lines were purchased from American Type Culture Collection (ATCC). The cell lines were authenticated by STR-profiling and tested for mycoplasma contamination to ensure that they were mycoplasma-free. To induce hypoxic stress, the cells were cultured in a hypoxia incubator chamber (STEMCELL Technologies Inc., #27310).

Colorectal cells were transfected with small interfering RNAs (siRNAs, 50 nM) against human dehydrogenase and acetyltransferase-coding genes using MAX siRNA transfection reagent (Thermo Scientific Dharmacon Inc., USA), while nonspecific siRNA (siNC) was used as a negative control. All siRNAs were purchased from GenePharma Technology (Shanghai, China). siRNA sequences were listed in Appendix Table S1.

Antibodies against GDH1 acetylation at K503, K527, or K503/527 were custom designed and constructed by ABclonal Technology (Wuhan, China). Briefly, the acetyl-peptides AcK503-GDH1 (ISGA-SE$_{Ac}$KDIVHSG), AcK527-GDH1 (IMRTAM$_{Ac}$KYNLGL) and their respective control peptides without acetyl groups were first

synthesized. Then, New Zealand White (NZW) rabbits were immunized by intradermal injection of 500 μg of indicated polypeptides which were mixed with Freund's adjuvant to 2 ml volume. This process was repeated three times, and the dose was reduced to half in the fourth time. Serum samples were taken to test the titers of indicated antibodies at 2 weeks after the fourth immunization. The antibodies were purified and obtained by affinity chromatography.

Quantitative RT–PCR (qRT–PCR)

Total RNA was extracted with an RNA high-purity total RNA rapid extraction kit (QIAGEN). cDNA was prepared using a GoScript reverse transcription system (Promega). qRT–PCR was performed using SYBR PCR premixture (Promega) and an ABI 7500 fast system under the following conditions: 5 min at 95°C followed by 38 cycles at 95°C for 30 s, 60°C for 40 s, and 72°C for 1 min. Data were normalized to the expression of the control gene (β-actin) for each experiment. Data are presented as the mean ± SD of three independent experiments. The sequences of the primer pairs used for qRT–PCR were listed in Appendix Table S2.

Western blotting and antibodies

Western blot analysis was performed using standard protocols. An anti-β-actin (Merck, CAS: ABT264) antibody was used as a control for whole-cell lysates. Endogenous antibodies including HIF1α (Clone number: D1S7W, CAS: #36169), HIF2α (Clone number: E2N9W, CAS: #57921), EGLN1 (Clone number: D31E11, CAS: #4835), COX4 (Clone number: 3E11, CAS: #4850), p300 (Clone number: D8Z4E, CAS: #86377), AMPK (Clone number: D63G4, CAS: #5832), and Phospho-AMPK (Clone number: 40H9, CAS: #2535), GDH1 (Clone number: D9F7P, CAS: #12793), LaminB (Clone number: D9V6H, CAS: #13435), BCAT1 (Clone number: D4V2T, CAS: #16431), BCAT2 (Clone number: D8K3O, CAS: #79764), GOT1 (Clone number: E4A4O, CAS: #34423), GOT2 (CAS: #71692), GPT (CAS: AV45710) were purchased from Cell Signaling Technology. Antibodies including His-tag (Clone number: HIS.H8, CAS: ab18184), Pan-Methyl-Lysine (CAS: ab7315), Phospho-Ser/Thr (CAS: ab117253), Phospho-Tyrosine (Clone number: EPR16871, CAS: ab179530) were purchased from Abcam. Antibody IDH1/2 (CAS: sc-373816) was purchased from Santa Cruze. The dilution of these primary antibodies was 1:1,000. Tag antibodies against FLAG (CAS: AE005) or HA (CAS: A0208) and β-Tubulin (CAS: AC008) antibody were purchased from Abclonal (Wuhan, China) and used at a dilution of 1:5,000. IP and IB analyses were performed with the indicated antibodies.

Cell viability assay

HCT116 or SW480 cells with or without genetic modifications were plated in DMEM (10% FBS) under hypoxia or normoxia for the indicated times. Cells were collected at the indicated time points, and cell viability was determined by trypan blue staining.

PI/Annexin V

We measured the percentage of apoptotic cells under hypoxic stress as previously described (Shao *et al*, 2019).

Mass spectrometry analysis of GDH1-interacting proteins and GDH1 acetylation

GDH1-FLAG and its interacting proteins was enriched by immunoprecipitation with an antibody against the Flag tag. The proteins were eluted and separated using SDS–PAGE followed by Coomassie blue staining. The gel lane was dissected and subjected to in-gel digestion. Briefly, the gel was chopped into 1 mm^3 pieces and decoloured using 50 mM NH$_4$HCO$_3$ in 30% ACN under oscillation. Then, the gel was subjected to vacuum freeze lyophilization and alkylated using 10 mM TCEP+ 50 mM CAA in 50 mM NH$_4$HCO$_3$ at 95°C for 5 min. The supernatant was removed, and the gel was again subjected to vacuum freeze lyophilization. Then, the gel was treated with trypsin (20 ng/μl in 50 mM NH$_4$HCO$_3$) and incubated at 37°C for 16 h. The peptides were extracted three times in an ultrasonic water bath by 0.1% TFA in 90% ACN. The resulting peptides were subjected to vacuum freeze lyophilization, purified using C18 stage tips and then analyzed via liquid chromatography–tandem mass spectrometry (LC–MS/MS). Peptides were loaded and separated on a homemade microtip C18 column (ReproSil-Pur C18-AQ, 3 μm, 75 μm × 250 mm) on a nanoflow HPLC Easy-nLC 1000 system (buffer A, 0.1% FA in H$_2$O; buffer B, 0.1% FA in 100% ACN; Thermo Fisher Scientific). The LC gradient was set as follows: 2–4% B for 1 min; 4–30% B for 47 min; 30–45% B for 5 min; 45–90% B for 1 min; and 90% B for 6 min. MS data were collected via data-dependent acquisition in the profile mode on a Q Exactive mass spectrometer set as follows: MS1 resolution, 70,000 @ m/z 200; mass range, 300–1,600 m/z; AGC Target, 3e6; maximum IT, 50 ms; topN, 10. MS2 resolution, 17,500 @ m/z 200; normalized collision energy (NCE), 27%; isolation width (m/z), 1.6 m/z; AGC Target, 1e5; maximum IT, 120 ms; charge states include 2–5; dynamic exclusion, 30 s. The mass spectrometric data were analyzed using Proteome Discoverer 2.3 against the human Swiss-Prot database with carbamidomethyl cysteine set as a fixed modification and oxidized methionine, protein N-term acetylation and lysine acetylation set as variable modifications.

Lysine-acetylated GDH1 expression and purification

To obtain site-directed *GDH1-Ac*K, we constructed pET22b-*GDH1* encoding *GDH1* with a C-terminal 6×His tag. We cotransformed *E. coli* BL21 (DE3) cells with *pAcKRS* and pET22b-*GDH1* with a C-terminal 6×His tag. As described previously (Neumann *et al*, 2008), GDH1-AcKs were overexpressed in *E. coli* BL21 (DE3) following the addition of Ara and IPTG in the presence of ampicillin, chloramphenicol, 10 mM NAM and AcK. GDH1-AcKs were purified by Ni-NTA affinity chromatography, followed by gel-filtration chromatography with a Superdex 75. The purity of the preparations was assessed by SDS–PAGE, and the protein concentration was determined using a Bradford protein assay kit.

Measurement of reversible GDH1 activity and GDH1 enzyme kinetics

GDH1 activity associated with αKG production was measured at room temperature. GDH1 was immunoprecipitated from the lysates of CRC cells or purified from *E. coli* and subjected to GDH1 enzymatic activity assays in reaction buffer containing 100 mM Tris (pH

8.0), 50 mM L-Glu, and 1 mM NAD^+. The change in absorbance at 340 nm due to an increase in NADH was measured using a BioTek Synergy Neo Multi-Mode Plate Reader (BioTek, USA).

GDH1 activity associated with Glu production was measured at room temperature in reaction buffer containing 100 mM Tris (pH 8.0), 10 mM αKG, 5 mM NADH, and 500 μM NH_4Cl. The change in absorbance at 340 nm due to a decrease in NADH was measured using a BioTek Synergy Neo Multi-Mode Plate Reader (BioTek, USA).

The continuous change in absorbance at 340 nm due to an increase or decrease in NADH was used to calculate the Vmax of αKG or Glu, and the *Km* was determined by nonlinear regression analysis, which was performed using Prism 7 (GraphPad).

Measurement of αKG

The indicated cells were seeded into six-well plates, then collected and lysed, and the lysate was examined using an αKG Assay Kit (Abcam, αKG Assay kit (colorimetric), CA, USA) according to the manufacturer's instructions.

Luciferase reporter assay

Transcriptional activation of HIF1α in HCT116 cells was measured as previously described (Wang *et al*, 2017). Relative levels of luciferase activity were normalized to the levels in untreated HCT116 cells expressing control vector and then normalized to the levels of luciferase activity induced by the Renilla control plasmid.

HIF peptide hydroxylation assay for assessing EGLN1 activity

An N-terminally biotinylated peptide corresponding to HIF1 residues 556–575 (DLDLEALAPYI PADDDFQLR) was synthesized by changing two methionines (M) to alanine (A). Equal amounts of HA-EGLN1 protein (10 nM) in HA beads were purified from the indicated HCT116 cells under hypoxia and incubated with the above peptide (100 nM) for 2 h in PHA buffer containing $FeCl2$ (100 μM), ascorbate (2 mM), and αKG (50 μM). The HA agarose beads were washed three times with NETN (20 mM Tris–HCl [pH 8.0], 100 mM NaCl, 1 mM EDTA, 0.5% NP-40), and peptide hydroxylation was determined by LC–MS.

To measure GDH1 activity using αKG as a substrate and the consequence of αKG exhaustion in EGLN1, we first incubated His-GDH1 (including WT or mutant) with GST-EGLN1 (in the GST beads) in the adjusted buffer, changing 10 mM αKG to 500 μM (called high αKG) or 80 μM (called low αKG, which is likely close to the cytoplasmic αKG level under normal oxygen conditions) αKG. Then, EGLN1 was precold washed twice and incubated with HIF1α to assess EGLN1 activity.

Measurement of EGLN1-bound αKG

To assess EGLN1-bound αKG, we first developed a radiometric ^{14}C-αKG-EGLN1 binding assay. In detail, bead-bound HA-EGLN1 purified from the indicated HCT116 cells under hypoxia was washed with Tris-buffered saline (TBS) buffer (50 mM Tris, 150 mM NaCl [pH 7.5]), followed by incubation with 0.2 mCi ^{14}C-αKG for 30 min in TBS buffer. The beads were then washed with TBS buffer containing 1% NP-40. The bead-bound EGLN1 protein was eluted with 10 mg of HA peptides, and radioactivity was detected by liquid scintillation counting. We also developed another method for testing EGLN1-bound αKG using LC–MS. In detail, we enriched HA-EGLN1 from the indicated HCT116 cells under hypoxia and incubated HA-EGLN1 in TBS buffer containing 100 μM αKG. HA-EGLN1 beads were quickly washed with TBS buffer containing 1% NP-40 but not αKG. Then, HA-EGLN1 was digested using protease to release αKG from the EGLN1 protein, and the αKG quantity was measured via liquid chromatography–mass spectrometry (LC–MS). The above results were normalized based on the total protein concentration in each sample.

Subcellular fractionation analyses

HCT116 cells were harvested and washed three times with cold PBS. Cytosolic or mitochondrial fractions were prepared using a Nuclear/Cytosol Fraction Kit (Active Motif).

Isothermal titration calorimetry

Thermodynamic parameters of the binding of GDH1 WT, K503R, or K503Q to Glu or αKG were measured by isothermal titration calorimetry (ITC) assays using an ITC200 Microcalorimeter (MicroCal) at 25°C. GDH1 was expressed in *E. coli* and purified via His tag affinity purification. In all experiments, the initial injection of 0.5 ml of Glu or αKG solution was discarded to eliminate the effect of titrant diffusion across the syringe tip during the equilibration process, and each dataset consisted of 20 injections of 2 ml each of 1 mM Glu or αKG into the sample cell containing 250 ml of 0.05 mM GDH1. The heat of dilution was negligible in all cases. The binding constant and other thermodynamic parameters were determined by fitting the integrated titration data using the single binding site model via the nonlinear least-squares method, which was implemented in MicroCal Origin software (version 7.0).

In vitro acetyltransferase activity assay

FLAG-tagged p300 was purified from HCT116 cells and eluted with the FLAG peptide. p300 was quantified as 50 ng/μl, and we added GDH1 to the p300 acetyltransferase activity reaction system according to the manufacturer's instructions. The acetyltransferase activity was measured using a kit (ab204536).

Subcutaneous xenograft model

All mice were maintained under a 12-h light/dark cycle with free access to water and standard mouse chow in a specific-pathogen-free (SPF) facility, receiving humane care. All experimental procedures were performed in compliance with the Guide for the Care and Use of Laboratory Animals and approved by the Institutional Animal Care and Use Committee (IACUC) in Guangzhou University (Guangzhou, China, ethics approval: #gzhu2018039).

Briefly, 2×10^6 HCT116-derived stable cells were subcutaneously injected into the left dorsal region of randomized 6-week-old male athymic nude mice. After inoculation for 28 days, the mice were euthanized, and the tumors were dissected. Differences in the weight of xenograft tumors were statistically analyzed.

Statistical analysis

All results are presented as the mean ± standard deviation (SD), unless stated otherwise. Statistical analyses were performed using two tailed Student's *t*-test for two groups comparison, one-way or two-way analysis of variance (ANOVA) for multiple comparisons on GraphPad Prism version 8.3 (GraphPad Software, Inc.). About clinical patients, Mann–Whitney *U*-test was used for two groups comparison, Pearson's correlation analysis was used to calculate the regression and correlation, log-rank test was used to assess the patient survival curve. $P < 0.05$ was considered statistically significant. No statistical methods were applied to pre-evaluate sample size. The sample size was determined based on our experiences and similar with reported literature for specific experiments. No data were excluded from the analyses. All experiments were performed with at least three biologically independent samples or three biologically independent experiments. n values indicated biologically independent samples and experiments. Except the IHC scoring, the investigators were not blinded to allocation during experiments and outcome assessment for consistent of experimental procedures. For *in vivo* and *in vitro* assays, groups were randomly allocated.

Data availability

This study contains no data amenable to large-scale repository deposition.

Expanded View for this article is available online.

Author contributions

Xiongjun Wang: Resources; supervision; funding acquisition; writing – original draft; project administration; writing – review and editing. **Kunhua Hu:** Conceptualization; data curation; formal analysis; validation; investigation; methodology. **Yufeng Ding:** Resources; formal analysis; investigation; project administration; writing – review and editing. **Hongwen Zhu:** Data curation; software; formal analysis; validation; investigation; visualization; methodology. **Xiaoqian Jing:** Resources; formal analysis; validation; investigation; visualization. **Weiling He:** Resources; methodology. **Hua Yu:** Resources; formal analysis; supervision; validation; investigation; methodology; project administration.

Disclosure and competing interests statement

The authors declare that they have no conflict of interest.

References

Böğürcü N, Seidel S, Garvalov BK, Acker T (2018) Analysis of hypoxia and the hypoxic response in tumor xenografts. *Methods Mol Biol* 1742: 283–300

Brahimi-Horn MC, Chiche J, Pouysségur J (2007) Hypoxia and cancer. *J Mol Med (Berl)* 85: 1301–1307

Chaika NV, Gebregiworgis T, Lewallen ME, Purohit V, Radhakrishnan P, Liu X, Zhang B, Mehla K, Brown RB, Caffrey T *et al* (2012) MUC1 mucin stabilizes and activates hypoxia-inducible factor 1 alpha to regulate metabolism in pancreatic cancer. *Proc Natl Acad Sci USA* 109: 13787–13792

Choudhary C, Weinert BT, Nishida Y, Verdin E, Mann M (2014) The growing landscape of lysine acetylation links metabolism and cell signalling. *Nat Rev Mol Cell Biol* 15: 536–550

De Robertis M, Massi E, Poeta ML, Carotti S, Morini S, Cecchetelli L, Signori E, Fazio VM (2011) The AOM/DSS murine model for the study of colon carcinogenesis: from pathways to diagnosis and therapy studies. *J Carcinog* 10: 9

Geng H, Liu Q, Xue C, David LL, Beer TM, Thomas GV, Dai MS, Qian DZ (2012) HIF1α protein stability is increased by acetylation at lysine 709. *J Biol Chem* 287: 35496–35505

Hanahan D, Weinberg RA (2011) Hallmarks of cancer: the next generation. *Cell* 144: 646–674

Jin L, Li D, Alesi GN, Fan J, Kang HB, Lu Z, Boggon TJ, Jin P, Yi H, Wright ER *et al* (2015) Glutamate dehydrogenase 1 signals through antioxidant glutathione peroxidase 1 to regulate redox homeostasis and tumor growth. *Cancer Cell* 27: 257–270

Kaelin WG, Ratcliffe PJ (2008) Oxygen sensing by metazoans: the central role of the HIF hydroxylase pathway. *Mol Cell* 30: 393–402

Ke Q, Costa M (2006) Hypoxia-inducible factor-1 (HIF-1). *Mol Pharmacol* 70: 1469–1480

Koivunen P, Lee S, Duncan CG, Lopez G, Lu G, Ramkissoon S, Losman JA, Joensuu P, Bergmann U, Gross S *et al* (2012) Transformation by the (R)-enantiomer of 2-hydroxyglutarate linked to EGLN activation. *Nature* 483: 484–488

Lorenzo FR, Huff C, Myllymäki M, Olenchock B, Swierczek S, Tashi T, Gordeuk V, Wuren T, Ri-Li G, McClain DA *et al* (2014) A genetic mechanism for Tibetan high-altitude adaptation. *Nat Genet* 46: 951–956

Luo F, Liu X, Yan N, Li S, Cao G, Cheng Q, Xia Q, Wang H (2006) Hypoxia-inducible transcription factor-1alpha promotes hypoxia-induced A549 apoptosis via a mechanism that involves the glycolysis pathway. *BMC Cancer* 6: 26

Neumann H, Peak-Chew SY, Chin JW (2008) Genetically encoding N(epsilon)-acetyllysine in recombinant proteins. *Nat Chem Biol* 4: 232–234

Raffel S, Falcone M, Kneisel N, Hansson J, Wang W, Lutz C, Bullinger L, Poschet G, Nonnenmacher Y, Barnert A *et al* (2017) BCAT1 restricts αKG levels in AML stem cells leading to IDHmut-like DNA hypermethylation. *Nature* 551: 384–388

Semenza GL (2003) Targeting HIF-1 for cancer therapy. *Nat Rev Cancer* 3: 721–732

Shao J, Lu J, Zhu W, Yu H, Jing X, Wang YL, Wang X, Wang XJ (2019) Derepression of LOXL4 inhibits liver cancer growth by reactivating compromised p53. *Cell Death Differ* 26: 2237–2252

Stillman TJ, Baker PJ, Britton KL, Rice DW (1993) Conformational flexibility in glutamate dehydrogenase. Role of water in substrate recognition and catalysis. *J Mol Biol* 234: 1131–1139

Sullivan LB, Gui DY, Vander Heiden MG (2016) Altered metabolite levels in cancer: implications for tumour biology and cancer therapy. *Nat Rev Cancer* 16: 680–693

Tarhonskaya H, Rydzik AM, Leung IK, Loik ND, Chan MC, Kawamura A, McCullagh JS, Claridge TD, Flashman E, Schofield CJ (2014) Non-enzymatic chemistry enables 2-hydroxyglutarate-mediated activation of 2-oxoglutarate oxygenases. *Nat Commun* 5: 3423

Thaker AI, Shaker A, Rao MS, Ciorba MA (2012) Modeling colitis-associated cancer with azoxymethane (AOM) and dextran sulfate sodium (DSS). *J Vis Exp* https://doi.org/10.3791/4100

Wang X, Qiao Y, Xiao M, Wang L, Chen J, Lv W, Xu L, Li Y, Wang Y, Tan MD *et al* (2017) Opposing roles of acetylation and phosphorylation in LIFR-dependent self-renewal growth signaling in mouse embryonic stem cells. *Cell Rep* 18: 933–946

Wang X, Liu R, Qu X, Yu H, Chu H, Zhang Y, Zhu W, Wu X, Gao H, Tao B *et al* (2019a) α-ketoglutarate-activated NF-κB signaling promotes compensatory glucose uptake and brain tumor development. *Mol Cell* 76: 148–162

Wang Y, Bai C, Ruan Y, Liu M, Chu Q, Qiu L, Yang C, Li B (2019b) Coordinative metabolism of glutamine carbon and nitrogen in proliferating cancer cells under hypoxia. *Nat Commun* 10: 201

Wapenaar H, Dekker FJ (2016) Histone acetyltransferases: challenges in targeting bi-substrate enzymes. *Clin Epigenetics* 8: 59

Yang C, Sudderth J, Dang T, Bachoo RM, McDonald JG, DeBerardinis RJ (2009) Glioblastoma cells require glutamate dehydrogenase to survive impairments of glucose metabolism or Akt signaling. *Cancer Res* 69: 7986–7993

Zhang Y, Yu G, Chu H, Wang X, Xiong L, Cai G, Liu R, Gao H, Tao B, Li W *et al* (2018) Macrophage-associated PGK1 phosphorylation promotes aerobic glycolysis and tumorigenesis. *Mol Cell* 71: 201–215

Zhao S, Lin Y, Xu W, Jiang W, Zha Z, Wang P, Yu W, Li Z, Gong L, Peng Y *et al* (2009) Glioma-derived mutations in IDH1 dominantly inhibit IDH1 catalytic activity and induce HIF-1alpha. *Science* 324: 261–265

Expanded View Figures
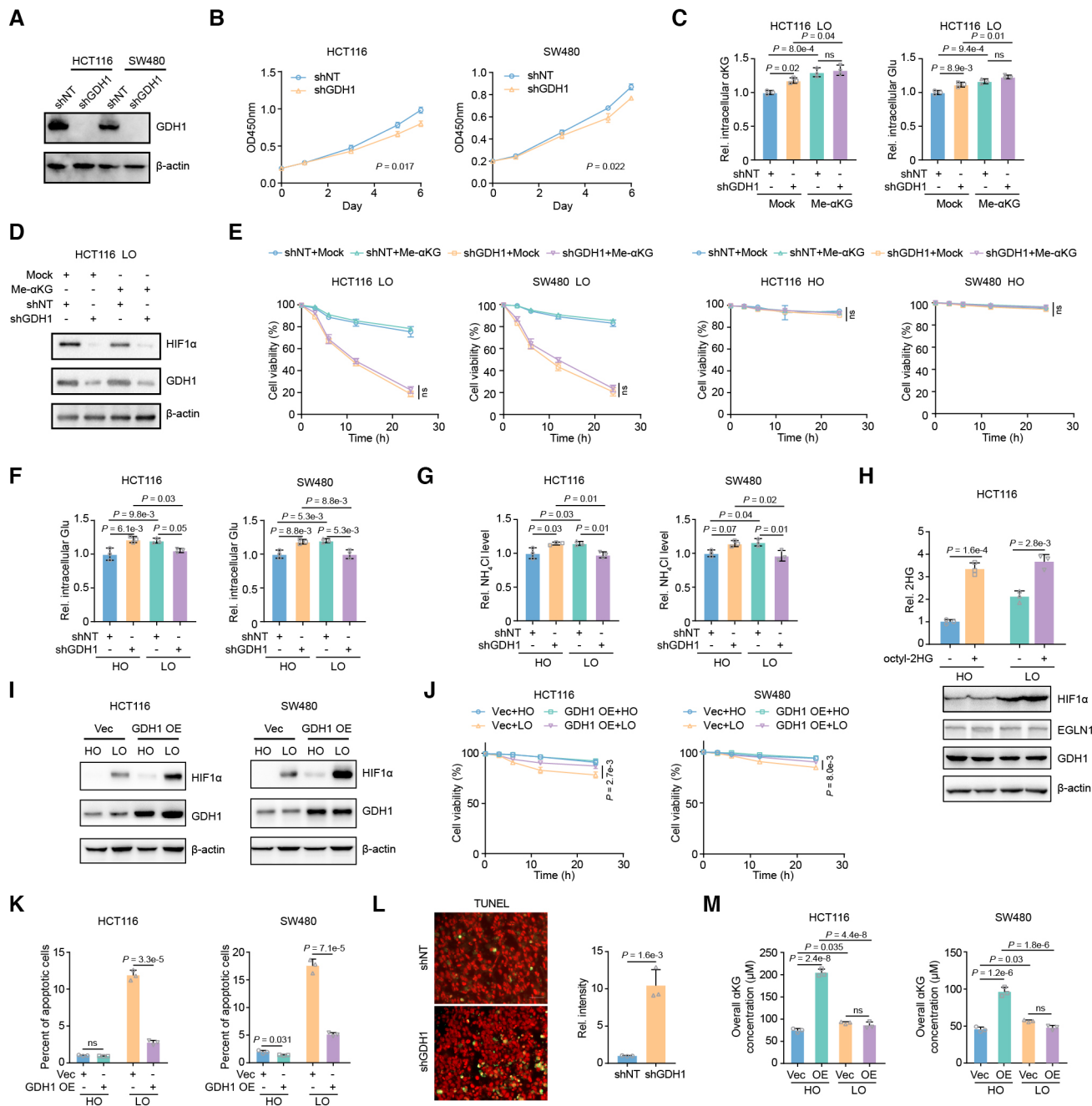
Figure EV1.

◀ **Figure EV1. GDH1 depletion sensitizes CRC cells to hypoxia.**

A   Construction of GDH1 depleted cell lines.
B   Cell proliferation assay was performed using cell lines constructed in Fig S1A ($n = 3$).
C, D HCT116 and SW480 cells with or without GDH1 were supplemented with cell permeable methyl-αKG under hypoxia. Then, the intracellular level of αKG was tested by αKG determination kit (C) ($n = 3$). Cells were collected and indicated antibodies were applied to test HIF1α, EGLN1 and GDH1 proteins (D).
E   HCT116 and SW480 cells with or without GDH1 were supplemented with cell permeable methyl-αKG under normoxia and hypoxia. Then, cell viability was counted by trypan blue staining ($n = 3$).
F, G HCT116 and SW480 cells with or without GDH1 were cultured under normoxia or hypoxia. Cells were collected for determining glutamate (Glu, F) and ammonia (NH_4Cl, G) ($n = 3$).
H   HCT116 were incubated with or without cell permeable octyl-2HG under normoxia or hypoxia. Indicated antibodies were applied to test HIF1α, EGLN1 and GDH1 proteins ($n = 3$).
I   HIF1α and GDH1 were tested by western blot in HCT116 or SW480 cells with Vec or GDH1 overexpression under normoxia and hypoxia.
J   HCT116 and SW480 cells with or without GDH1 overexpression were incubated under normoxia and hypoxia, respectively. Then, cell viability was counted by trypan blue staining ($n = 3$).
K   The apoptotic percent of cells in Fig S1D was counted by PI/Annexing V double staining ($n = 3$).
L   TUNEL analysis of GDH1 knockdown HCT116 cells under hypoxia. The left was the representative microscopic data, the right was the calculated relative intensity data ($n = 3$).
M   The overall αKG level in HCT116 or SW480 cells with or without GDH1 overexpression under normoxia and hypoxia ($n = 3$).

Data information: Data are mean ± SD from the biological replicates (B, C, E–H, J–M). Statistics: two-way ANOVA with Tukey's HSD *post hoc* test (B, E, J); one-way ANOVA with Tukey's HSD *post hoc* test (C, F–H, M); unpaired two-tailed Student's *t*-test (K, L).
Source data are available online for this figure.
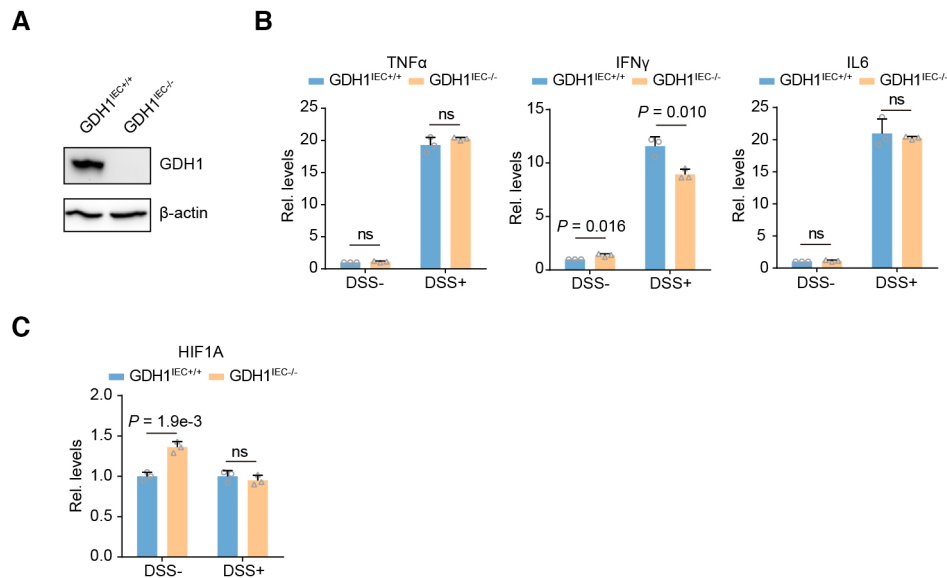
Figure EV2. GDH1 depletion did not significantly affect cytokine and HIF1A expression.

A   The identification of GDH1 knock out in the intestine by western blot.
B   qRT-PCR analysis of whole colon homogenates to assess cytokines production after AOM/DSS treatment ($n = 3$).
C   qRT-PCR analysis of whole colon homogenates to assess HIF1A expression after AOM/DSS treatment ($n = 3$).

Data information: Data are mean ± SD from the biological replicates (B, C). Statistics: unpaired two-tailed Student's *t*-test (B, C).
Source data are available online for this figure.
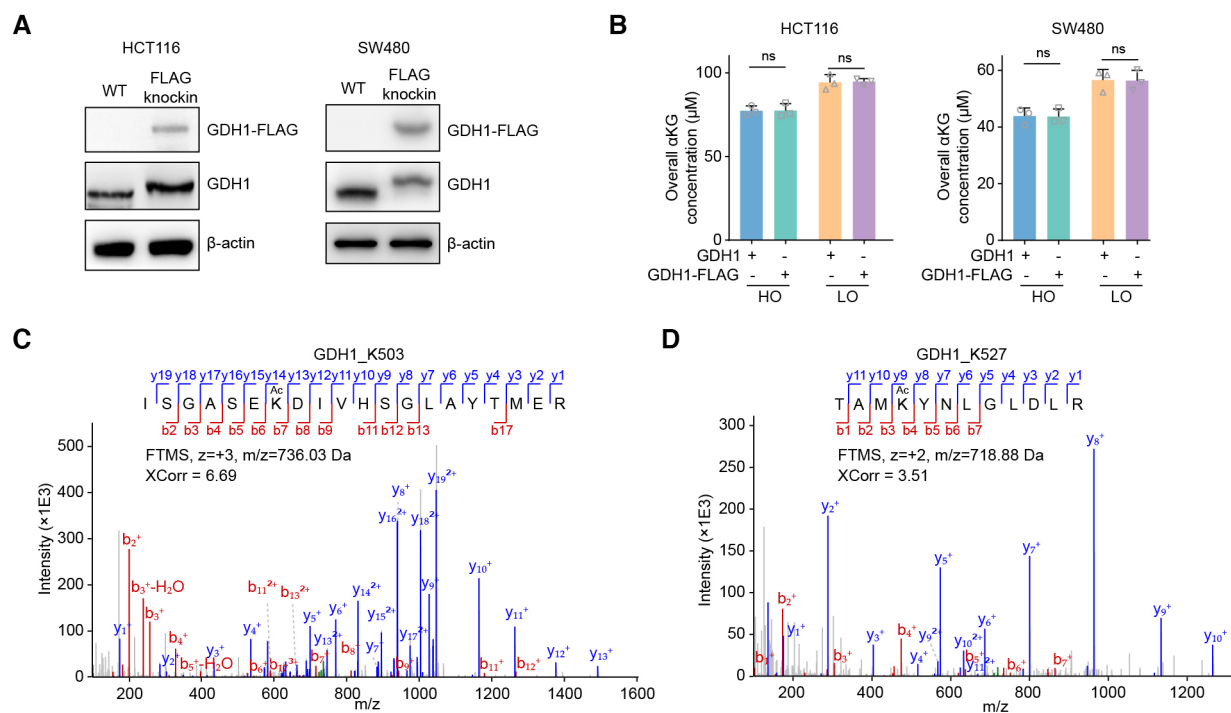
Figure EV3. The enrichment of GDH1 for acetylation identification.

A   The successful knockin of FLAG into C terminal of GDH1 in HCT116 or SW480 cells was tested by western blot.

B   The overall αKG level in HCT116 or SW480 cells with or without FLAG tagging endogenous GDH1 C terminal under normoxia and hypoxia (*n* = 3).

C, D   MS/MS spectra identified K503 and K527 acetylation of GDH1 purified from HCT116 cells.

Data information: Data are mean ± SD from the biological replicates (B). Statistics: unpaired two-tailed Student's *t*-test (B).
Source data are available online for this figure.
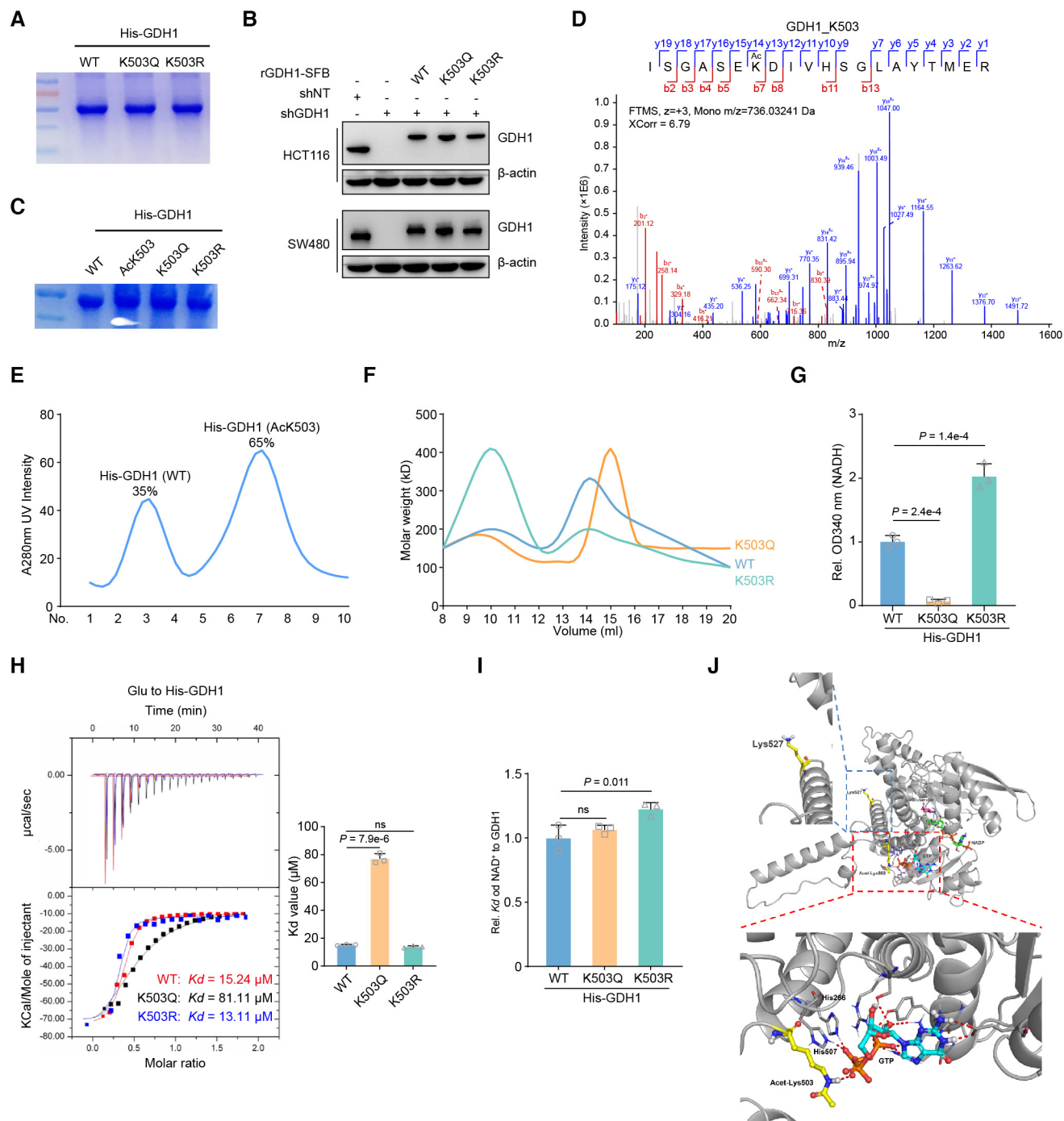
Figure EV4.

Figure EV4. GDH1-K503 acetylation modulates its enzyme activity.

A His-GDH1 (including WT, K503Q and K503R mutants) were purified from *E. coli* and separated by SDS-PAGE. The coomassie blue staining was shown.
B Construction of GDH1-depleted cell lines, which were rescued with expression of WT GDH1 or K503Q, or K503R mutant GDH1.
C His-GDH1 (including WT, AcK503, K503Q and K503R mutants) were purified from *E. coli* and separated by SDS-PAGE. The coomassie blue staining was shown.
D The acetyl modification of AcK503 His-GDH1 from *E. coli* was confirmed by LC–MS/MS.
E His-GDH1 (including WT and AcK503) purified from *E. coli* were separated and analyzed by FPLC.
F His-GDH1 (including WT and AcK503) purified from *E. coli* were analyzed by dynamic light scattering.
G Measure the NADH level by the OD340 absorbance value, respectively ($n = 3$).
H His-GDH1 proteins (including WT, K503Q or K503R) were purified from *E. coli* to determine Kd value. ITC assays were performed with precipitated His-GDH1 proteins and αKG ($n = 3$)
I ITC assays were performed with precipitated His-GDH1 proteins and NAD$^+$ ($n = 3$)
J The complex of GDH1 (PDB code: 4ED5) with GTP is superimposed on the GDH1-GTP complex. The protein and metabolites are shown as cartoon and are colored gray and orange or yellow, respectively. Acetyl-K503, K527 and GTP are shown as sticks.

Data information: Data are mean ± SD from the biological replicates (G–I). Statistics: one-way ANOVA with Tukey's HSD *post hoc* test (G–I).
Source data are available online for this figure.
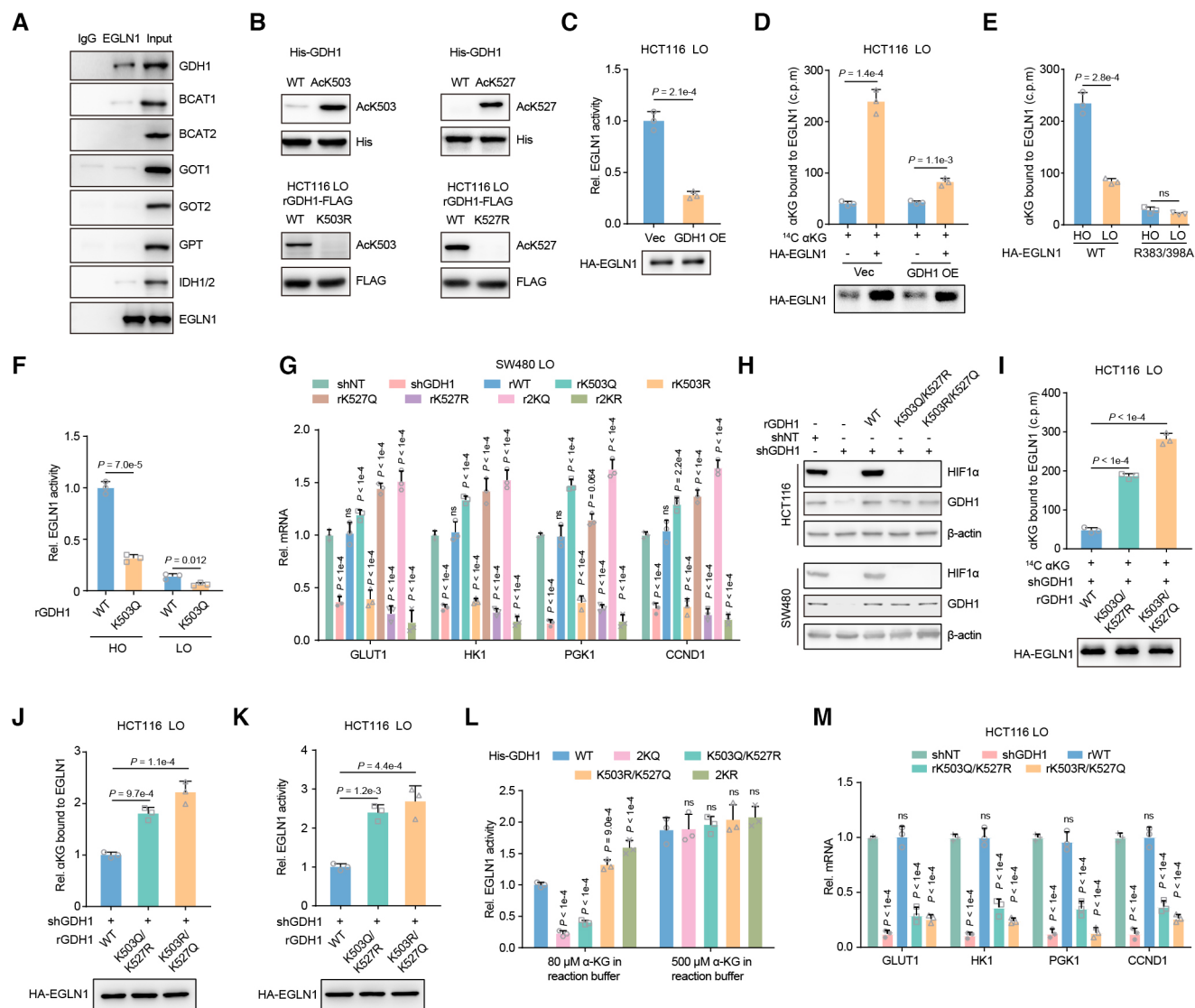
Figure EV5.

◀

Figure EV5. Acetylation modification at both K503 and K527 regulates the survival of CRC cells under hypoxia.

A   EGLN1 was enriched from hypoxia pretreated HCT116 cells and indicated antibodies were applied to test the association of EGLN1 with αKG producing or consuming metabolic enzymes.

B   The specificity of antibodies against GDH1-AcK503 or -AcK527 was analyzed by western blot. His- GDH1-AcK503 or -AcK527 was prepared from *E. coli*. Restored expression of GDH1-FLAG (including WT, K503R and K527R) was enriched from HCT116 cells.

C   HA-EGLN1 was enriched from HCT116 cells with or without GDH1 overexpression under hypoxia and then EGLN1 activity was tested by converting αKG to succinate ($n = 3$).

D   Relative αKG in EGLN1. HA-EGLN1 was enriched from Vec or GDH1 OE cells under hypoxia. A radiometric 14C-αKG-EGLN1 binding assay was performed using HA-EGLN1 incubating with 14C-αKG ($n = 3$).

E   Negative control used for testing relative αKG in EGLN1. HA-EGLN1 (including WT and R383/398A mutant) was enriched from HCT116 under normoxia and hypoxia. A radiometric 14C-αKG-EGLN1 binding assay was performed using HA-EGLN1 incubating with 14C-αKG ($n = 3$).

F   Measure the relative EGNL1 activity affected by restored WT or K503Q GDH1 under normoxia or hypoxia *in vitro* ($n = 3$).

G   The mRNA expression of HIF1α target genes, GLUT1, HK1, PGK1 and CCND1 was tested in indicated cell lines ($n = 3$).

H   Detection of HIF1α protein stability in GDH1 depleted cell lines which were rescued with expression of WT GDH1 or K503Q/K527R or K503R/K527Q mutant GDH1.

I, J   Relative αKG in EGLN1. HA-EGLN1 was enriched from indicated cells under hypoxia. A radiometric 14C-αKG-EGLN1 binding assay was performed using HA-EGLN1 incubating with 14C-αKG (H). EGLN1 was digested by trypsin and LC–MS was applied to detect αKG eluted from EGLN1 (I) ($n = 3$).

K   HA-EGLN1 was enriched from indicated genetic manipulated HCT116 cells under hypoxia and then EGLN1 activity was tested by converting αKG to succinate ($n = 3$).

L   HA-EGLN1 was enriched from HCT116 cells under hypoxia and then incubated with indicated His-GDH1 in the buffer containing 80 or 500 μM αKG. EGLN1 activity was tested by converting αKG to succinate ($n = 3$).

M   The mRNA expression of HIF1α target genes, GLUT1, HK1, PGK1 and CCND1, in indicated cell lines ($n = 3$).

Data information: Data are mean ± SD from the biological replicates (C–G, I–M). Statistics: unpaired two-tailed Student's *t*-test (C–F); one-way ANOVA with Tukey's HSD *post hoc* test (G, I–M).

Source data are available online for this figure.

TABLE OF CONTENTS

Appendix Figures and Figure legends

Appendix Tables and Table legends

Appendix Figures and Figure legends

Appendix Figure S1. p300 is localized in both the cytosol and nucleus.

(A) The knockdown efficiency of siRNA targeting PCAF, TIP60, CBP and p300 in HCT116 cells was analyzed by qRT-PCR. Data represent the mean ± SD (unpaired two-tailed student's t-test, n=3).

(B) The cellular localization of the interactors of p300 from Biogrid database.

(C) Immunofluorescence of p300 in HCT116 and SW480 cells was performed to analyze p300 localization. DAPI indicates nuclei location.

(D) Immunoblot of HIF1α protein level in the NC or siP300 groups when overexpressing WT- or 2KQ-GDH1.
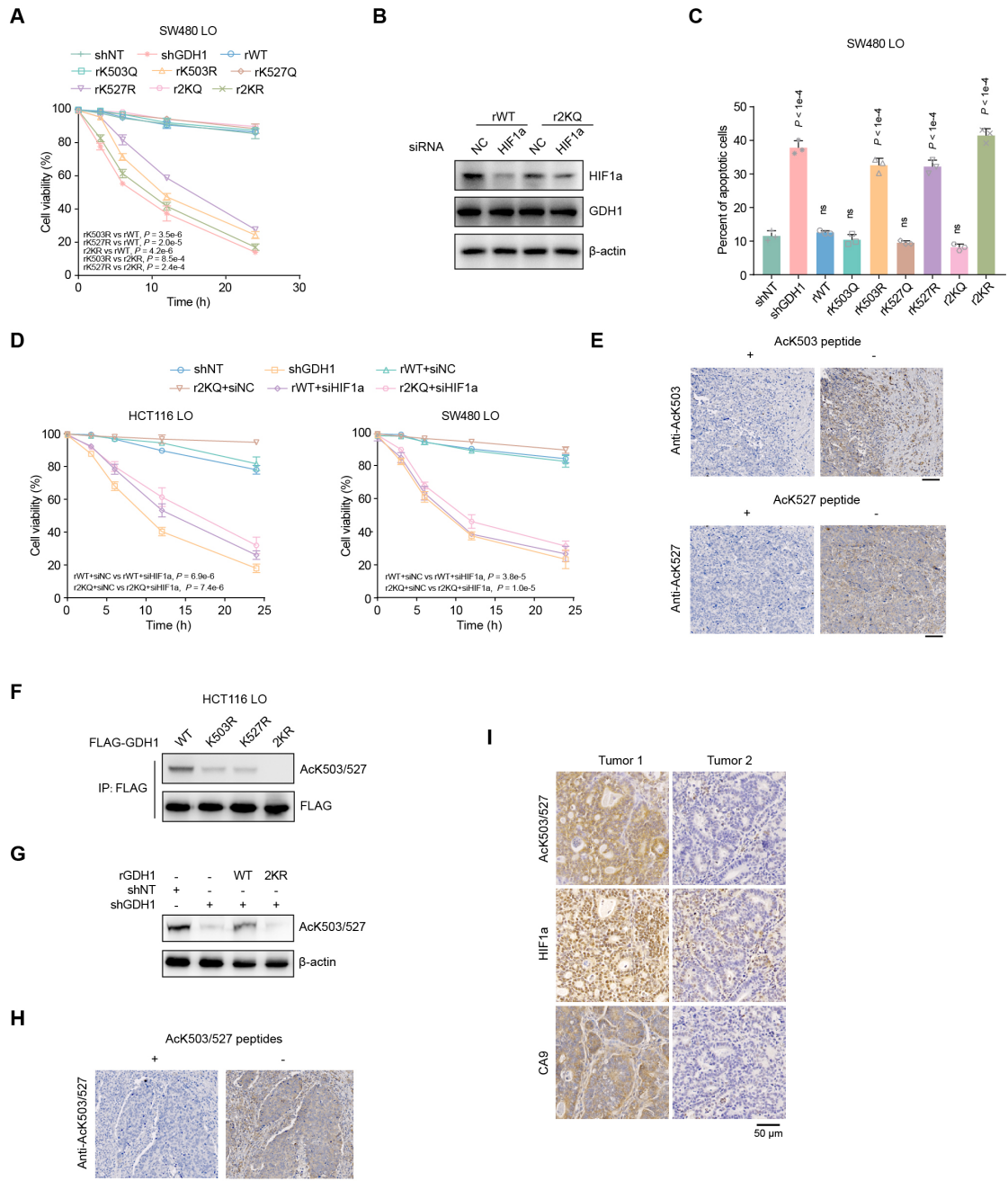
Appendix Figure S2. GDH1 acetylation at both K503 and K527 increased resistance of CRC cell to hypoxia

(A) Cell viability percent of indicated cell lines under hypoxia was analyzed by trypan blue and PI/Annexing V double staining, respectively. Mean ± SD, two-way ANOVA with Tukey's HSD post hoc test, n=3.

(B) Immunoblot of HIF1α protein level in the NC or siHIF1α groups when overexpressing WT- or 2KQ-GDH1.

(C) Cell apoptotic percent of indicated cell lines under hypoxia was analyzed by trypan blue and

PI/Annexing V double staining, respectively. Mean ± SD, one-way ANOVA with Tukey's HSD post hoc test, n=3.

(D) Cell viability of indicated cell lines under hypoxia was analyzed by trypan blue and PI/Annexing V double staining, respectively. Mean ± SD, two-way ANOVA with Tukey's HSD post hoc test.

(E) Validation of the specificity of antibodies against AcK503 and AcK507 in IHC. IHC analyses of human CRC tissues were performed with the indicated antibodies in the presence (+) or absence (-) of specific blocking peptides.

(F-G) Western blot analysis of the specificity of antibody against GDH1-AcK503/527.

(H) Validation of the specificity of antibody against AcK503/527 in IHC. IHC analyses of human CRC tissues were performed with the indicated antibodies in the presence (+) or absence (-) of specific blocking peptides.

(I) The representative images were shown after antibodies against GDH1-AcK503/527 and HIF1α were stained in the tumor tissues from AOM/DSS CRC samples.

Appendix Tables and Table legends

Appendix Table S1. siRNA sequence used in this study. Related to Methods.

Human Gene	siRNA sequences (5'-3', sense)	siRNA sequences (5'-3', anti-sense)
siRNA sequences against 163 dehydrogenases		
AASDH-1	UUAAUGCUGCUUCUGAAUUAU	AUAAUUCAGAAGCAGCAUUAA
AASDH-2	UGUGCAGUUACAUGGUAUAAU	AUUAUACCAUGUAACUGCACA
AASDH-3	GGUCACCUGCAGUGGAAAUUU	AAAUUUCCACUGCAGGUGACC
AASDHPPT-1	CGUCUGAUGAUAAGGAAAUUA	UAAUUUCCUUAUCAUCAGACG
AASDHPPT-2	GCAAGUUGGAAUUGAUAUAAU	AUUAUAUCAAUUCCAACUUGC
AASDHPPT-3	GAUAUAGGCCAAGUUUAUAAA	UUUAUAAACUUGGCCUAUAUC
ACAD10-1	UAUCCCUUCUGGAACUAUAUU	AAUAUAGUUCCAGAAGGGAUA
ACAD10-2	UGCAGUCUUGAGCAAUAAUUU	AAAUUAUUGCUCAAGACUGCA
ACAD10-3	UUGGAUAUAGCCAUGAUUAAA	UUUAAUCAUGGCUAUAUCCAA
ACAD11-1	GUCGAAUCUUCCGUGAUUUAA	UUAAAUCACGGAAGAUUCGAC
ACAD11-2	GAUAUCUUCUGGGAAAUAAUU	AAUUAUUUCCCAGAAGAUAUC
ACAD11-3	AGACUGACAGCCAAGAUAUAA	UUAUAUCUUGGCUGUCAGUCU
ACAD8-1	CCGAGAGAUGGCUCCAAAUAU	AUAUUUGGAGCCAUCUCUCGG
ACAD8-2	ACCAGCACCACAGCCUAUAUA	UAUAUAGGCUGUGGUGCUGGU
ACAD8-3	GAGGAACAGAGGCACAAAUUU	AAAUUUGUGCCUCUGUUCCUC
ACAD9-1	AUGGAGGACUGGCCAAUAUUU	AAAUAUUGGCCAGUCCUCCAU
ACAD9-2	GGGAAACCCGAAGAUAAAUUA	UAAUUUAUCUUCGGGUUUCCC
ACAD9-3	GGAUUGAUUCAGGAGAAAUUU	AAAUUUCUCCUGAAUCAAUCC
ACADL-1	GGACUGCUUGGUGUCAAUAUU	AAUAUUGACACCAAGCAGUCC
ACADL-2	CAGACAGUGCAACAUAAAUUA	UAAUUUAUGUUGCACUGUCUG
ACADL-3	UGGUGGUACAAAUGAAAUAAU	AUUAUUUCAUUUGUACCACCA
ACADM-1	UCAAGCUACUGCUCGUAAAUU	AAUUUACGAGCAGUAGCUUGA
ACADM-2	AGAUUGGGAGAAAGGAAUUAA	UUAAUUCCUUUCUCCCAAUCU
ACADM-3	UUGGAGGCAAUGGAUUUAAUA	UAUUAAAUCCAUUGCCUCCAA
ACADS-1	UUGCCGAGAAGGAGUUGUUUC	GAAACAACUCCUUCUCGGCAA
ACADS-2	GCGACUCAUGGGUUCUGAAUG	CAUUCAGAACCCAUGAGUCGC
ACADS-3	GCUGCCAUGCUGAAGGAUAAC	GUUAUCCUUCAGCAUGGCAGC
ACADSB-1	UCAGAAGCUCUACUCAAUAUA	UAUAUUGAGUAGAGCUUCUGA
ACADSB-2	UGAUAAAGAGGGAGAUUAUUA	UAAUAAUCUCCCUCUUUAUCA
ACADSB-3	GACUACACUAUUCCAUAUAUU	AAUAUAUGGAAUAGUGUAGUC
ACADVL-1	AGAGCAGACACAGUUUCUUAA	UUAAGAAACUGUGUCUGCUCU
ACADVL-2	GCGGUAGAUCAUGCCACUAAU	AUUAGUGGCAUGAUCUACCGC
ACADVL-3	GGUGGAGGCCAAGCUGAUAAA	UUUAUCAGCUUGGCCUCCACC
ADH1A-1	GGCCCAUGAAGUUCGUAUUAA	UUAAUACGAACUUCAUGGGCC
ADH1A-2	GACAUCAACAAGGACAAAUUU	AAAUUUGUCCUUGUUGAUGUC
ADH1A-3	GCUAUUCUUGGUGGCUUUAAA	UUUAAAGCCACCAAGAAUAGC
ADH1B-1	GACAUCAACAAGGACAAAUUU	AAAUUUGUCCUUGUUGAUGUC
ADH1B-2	UUCCCAGAACCUCUCAAUAAA	UUUAUUGAGAGGUUCUGGGAA

ADH1B-3	UUUCACUGGAUGCGUUAAUAA	UUAUUAACGCAUCCAGUGAAA
ADH1C-1	GACAUCAACAAGGACAAAUUU	AAAUUUGUCCUUGUUGAUGUC
ADH1C-2	UUCCCAGAACCUCUCAAUAAA	UUUAUUGAGAGGUUCUGGGAA
ADH1C-3	UUUCACUGGAUGCAUUAAUAA	UUAUUAAUGCAUCCAGUGAAA
ADH4-1	CAUCUAUUCUCCAGCAAUUAU	AUAAUUGCUGGAGAAUAGAUG
ADH4-2	UCUGAGUCCACUCACAAAUUU	AAAUUUGUGAGUGGACUCAGA
ADH4-3	AUAAUCGGCCGUACUAUAAAU	AUUUAUAGUACGGCCGAUUAU
ADH5-1	CAGUGUGGAGAAUGCAAAUUU	AAAUUUGCAUUCUCCACACUG
ADH5-2	UGGAGCCACUGAAUGUAUUAA	UUAAUACAUUCAGUGGCUCCA
ADH5-3	CGAACUGUUGUAAAGAUUUAA	UUAAAUCUUUACAACAGUUCG
ADH6-1	UAGAGAAAGUAUGCCUAAUUA	UAAUUAGGCAUACUUUCUCUA
ADH6-2	CUAAACUGGUUGCUGAUUAUA	UAUAAUCAGCAACCAGUUUAG
ADH6-3	CAAUGAAGCAGUUGAAUUAAU	AUUAAUUCAACUGCUUCAUUG
ADH7-1	UUUGCAUUAGGAGCGAUAUUA	UAAUAUCGCUCCUAAUGCAAA
ADH7-2	GACCUCAACAAAGACAAAUUU	AAAUUUGUCUUUGUUGAGGUC
ADH7-3	GAGUUCCUGGCAAAGAAAUUU	AAAUUUCUUUGCCAGGAACUC
ADHFE1-1	UGAGAUGGCUGUUUCAAAUAU	AUAUUUGAAACAGCCAUCUCA
ADHFE1-2	GGUUUAGUGAAGAUGUAUAAA	UUUAUACAUCUUCACUAAACC
ADHFE1-3	GCUUCAAUGAAACUGUAUUAA	UUAAUACAGUUUCAUUGAAGC
ALDH16A1-1	GGCAGCCAGGAUGGCAUUUAA	UUAAAUGCCAUCCUGGCUGCC
ALDH16A1-2	UGGGAGCCCAUGGGAGUAAUU	AAUUACUCCCAUGGGCUCCCA
ALDH16A1-3	GUCCAGGCCAUGUGGUAUUUC	GAAAUACCACAUGGCCUGGAC
ALDH18A1-1	CUGAGCAGAGAGCAGAAAUUA	UAAUUUCUGCUCUCUGCUCAG
ALDH18A1-2	UCUGCUCAGGACACCAUUAUU	AAUAAUGGUGUCCUGAGCAGA
ALDH18A1-3	CUCAGAGCAUGGAAGUUUAAA	UUUAAACUUCCAUGCUCUGAG
ALDH1A-11	UCAGUGAGUGGCAAGAAAUUU	AAAUUUCUUGCCACUCACUGA
ALDH1A1-2	CUCCACGUGGCAUCUUUAAUA	UAUUAAAGAUGCCACGUGGAG
ALDH1A1-3	CAGCAAAUCAUGAAGUUUAAA	UUUAAACUUCAUGAUUUGCUG
ALDH1A2-1	AGUACACCAAGAUCUUUAUAA	UUAUAAAGAUCUUGGUGUACU
ALDH1A2-2	UGGCAAUACAGUAGUUAUUAA	UUAAUAACUACUGUAUUGCCA
ALDH1A2-3	UUGGCCCUGUUCAGGAAAUUU	AAAUUUCCUGAACAGGGCCAA
ALDH1A3-1	UCAAGUUCACCAAGAUAUUUA	UAAAUAUCUUGGUGAACUUGA
ALDH1A3-2	CUUCAACUCGGGAGCAAAUAU	AUAUUUGCUCCCGAGUUGAAG
ALDH1A3-3	GCUCCAUUUGGUGGCUUUAAA	UUUAAAGCCACCAAAUGGAGC
ALDH1B1-1	CACGCCAUUUGGAGGGUUUAA	UUAAACCCUCCAAAUGGCGUG
ALDH1B1-2	ACCAGCUGUUCAUCAACAAUG	CAUUGUUGAUGAACAGCUGGU
ALDH1B1-3	AGCACGUGGAUGUUGACAAAG	CUUUGUCAACAUCCACGUGCU
ALDH1L1-1	AUGCUGCUGGUGAAGAAUAUU	AAUAUUCUUCACCAGCAGCAU
ALDH1L1-2	GUUUGCAGAGCUGACAUUAAA	UUUAAUGUCAGCUCUGCAAAC
ALDH1L1-3	GACCCUCAUUCACGGAGAUAA	UUAUCUCCGUGAAUGAGGGUC
ALDH1L2-1	GUUCAUUCCCAUGGAUAUAAU	AUUAUAUCCAUGGGAAUGAAC
ALDH1L2-2	GGAGAACCACUGGAAAUUAAA	UUUAAUUUCCAGUGGUUCUCC
ALDH1L2-3	CGGUGUCUGUGCCAUUAUUAU	AUAAUAAUGGCACAGACACCG

ALDH2-1	CUCAAAUGUCUCCGGUAUUAU	AUAAUACCGGAGACAUUUGAG
ALDH2-2	AGGUCUUCUGCAACCAGAUUU	AAAUCUGGUUGCAGAAGACCU
ALDH2-3	GAUUUGGACAAGGCCAAUUAC	GUAAUUGGCCUUGUCCAAAUC
ALDH3A1-1	CAAGGAUCUGUACCCAGUAAU	AUUACUGGGUACAGAUCCUUG
ALDH3A1-2	GGGACUAUGGAAGAAUCAUUA	UAAUGAUUCUUCCAUAGUCCC
ALDH3A1-3	AGCAACGACAAGGUGAUUAAG	CUUAAUCACCUUGUCGUUGCU
ALDH3A2-1	CAGGAAAUGCUGUGAUUAUAA	UUAUAAUCACAGCAUUUCCUG
ALDH3A2-2	AUGUAGAUGAGGCCAUAAAUU	AAUUUAUGGCCUCAUCUACAU
ALDH3A2-3	UCAGCGUCCCUGUUUAUUAAA	UUUAAUAAACAGGGACGCUGA
ALDH3B1-1	UGCUGAAGCCAUCGGAGAUUA	UAAUCUCCGAUGGCUUCAGCA
ALDH3B1-2	UCGUGUGGGCAAGAUUGUUAU	AUAACAAUCUUGCCCACACGA
ALDH3B1-3	GCACCAUCACCCGUUUCUAUG	CAUAGAAACGGGUGAUGGUGC
ALDH3B2-1	CCUCCGGCCUGGAGAAAUUAA	UUAAUUUCUCCAGGCCGGAGG
ALDH3B2-2	GGUGCUGAAGCCGUCAGAAAU	AUUUCUGACGGCUUCAGCACC
ALDH3B2-3	AUGAGGGCUUCACCUACAUAU	AUAUGUAGGUGAAGCCCUCAU
ALDH4A1-1	GGUCAUCAAGGAGACACAUAA	UUAUGUGUCUCCUUGAUGACC
ALDH4A1-2	ACAAGAGCCUGCUCAACAAAG	CUUUGUUGAGCAGGCUCUUGU
ALDH4A1-3	AGGAGCACAGUCGGAUCAAAG	CUUUGAUCCGACUGUGCUCCU
ALDH5A1-1	CUUCGGAAGUGGUACAAUUUA	UAAAUUGUACCACUUCCGAAG
ALDH5A1-2	GGGCCAUGGCAUCUAAAUUUA	UAAAUUUAGAUGCCAUGGCCC
ALDH5A1-3	GGCGUCAACGAAGGAUUAAUU	AAUUAAUCCUUCGUUGACGCC
ALDH6A1-1	GGGCAGACACUUCAGUAUUAA	UUAAUACUGAAGUGUCUGCCC
ALDH6A1-2	CCAAAGACAUGGACCUUUAUU	AAUAAAGGUCCAUGUCUUUGG
ALDH6A1-3	AGCCAUCCAGAUUGUAAAUAA	UUAUUUACAAUCUGGAUGGCU
ALDH7A1-1	GUGGCUGUCACAAAGAUAAUA	UAUUAUCUUUGUGACAGCCAC
ALDH7A1-2	ACUGCGAGGCGACUGUUUAUA	UAUAAACAGUCGCCUCGCAGU
ALDH7A1-3	CGAUUCUCUAUGUCUUUAAAU	AUUUAAAGACAUAGAGAAUCG
ALDH8A1-1	UUACCUUGUAGCUCAUAUAUA	UAUAUAUGAGCUACAAGGUAA
ALDH8A1-2	CCACCAGGUGUGGUCAAUAUU	AAUAUUGACCACACCUGGUGG
ALDH8A1-3	UUGCUGAAGGUGCCCAAAUUU	AAAUUUGGGCACCUUCAGCAA
ALDH9A1-1	UUGGAGGCUGCCAGGAUAAUA	UAUUAUCCUGGCAGCCUCCAA
ALDH9A1-2	GUUAUGUGGUGGAGAUAUAUA	UAUAUAUCUCCACCACAUAAC
ALDH9A1-3	GUGUGACAAUCGAAUAUUAUU	AAUAAUAUUCGAUUGUCACAC
BCKDHA-1	CUCGGCGGAGUUUAUAGAUAA	UUAUCUAUAAACUCCGCCGAG
BCKDHA-2	GCUCGGUGGAUGAGGUCAAUU	AAUUGACCUCAUCCACCGAGC
BCKDHA-3	AGGUCAAUUACUGGGAUAAAC	GUUUAUCCCAGUAAUUGACCU
BCKDHB-1	AGAUCCUACUGCAGUAAUAUU	AAUAUUACUGCAGUAGGAUCU
BCKDHB-2	GUUGGCUUGCGAGACAAAUAU	AUAUUUGUCUCGCAAGCCAAC
BCKDHB-3	AUUGAUCUGAGGACUAUAAUA	UAUUAUAGUCCUCAGAUCAAU
BCKDK-1	UGCACGUGCAUGAGCUAUAUA	UAUAUAGCUCAUGCACGUGCA
BCKDK-2	CUCUCACCAAAGAAGAUUAUU	AAUAAUCUUCUUUGGUGAGAG
BCKDK-3	GCACGUGCAUGAGCUAUAUAU	AUAUAUAGCUCAUGCACGUGC
BDH1-1	UGGAGCAAGACGCCCACUAUU	AAUAGUGGGCGUCUUGCUCCA

BDH1-2	CAAGGAGCUGGACAGCCUAAA	UUUAGGCUGUCCAGCUCCUUG
BDH1-3	ACUACGGCAAGAAGUACUUUG	CAAAGUACUUCUUGCCGUAGU
BDH2-1	GUCAUAGCCACAGACAUUAAU	AUUAAUGUCUGUGGCUAUGAC
BDH2-2	AGACUUGAUGUUCUCUUUAAU	AUUAAAGAGAACAUCAAGUCU
BDH2-3	UCAGAAAUCUGGCAAUAUUAU	AUAAUAUUGCCAGAUUUCUGA
CHDH-1	UGAAGCUCACCAGAGAAAUUU	AAAUUUCUCUGGUGAGCUUCA
CHDH-2	CUUGUGAGCAGGGUGCUAUUU	AAAUAGCACCCUGCUCACAAG
CHDH-3	AGAGAAGGCAGCUGACAUUAU	AUAAUGUCAGCUGCCUUCUCU
D2HGDH-1	GCCUGCGGUUUCUUCGAUAUG	CAUAUCGAAGAAACCGCAGGC
D2HGDH-2	AUGGUAACCUGCACCUCAAUG	CAUUGAGGUGCAGGUUACCAU
D2HGDH-3	GGUGAGAUCCUGUCUGCAUUC	GAAUGCAGACAGGAUCUCACC
DHDH-1	GGCAGAAGCCAGAGAAGAUUU	AAAUCUUCUCUGGCUUCUGCC
DHDH-2	CGAAGGAGUUUGCACAGAAAC	GUUUCUGUGCAAACUCCUUCG
DHDH-3	AUCCCGAGCCCUCUUCCUUAU	AUAAGGAAGAGGGCUCGGGAU
DHODH-1	UGAGAGUUCUGGGCCAUAAAU	AUUUAUGGCCCAGAACUCUCA
DHODH-2	CAUUAACAGGUAUGGAUUUAA	UUAAAUCCAUACCUGUUAAUG
DHODH-3	CAAGGCCGAGUUCCCAUAAUU	AAUUAUGGGAACUCGGCCUUG
DHRS1-1	CGUGUGCCCAAGUGGAUUAUU	AAUAAUCCACUUGGGCACACG
DHRS11-1	UACAGAUGUGACCUAUCAAAU	AUUUGAUAGGUCACAUCUGUA
DHRS11-2	UGGACGAUGGGCACAUCAUUA	UAAUGAUGUGCCCAUCGUCCA
DHRS11-3	AGGUGUGGUGGAGACACAAUU	AAUUGUGUCUCCACCACACCU
DHRS1-2	CAAAGCAGGCGCCACAGUUUA	UAAACUGUGGCGCCUGCUUUG
DHRS12-1	CCCAAGCAAAUCUGGAAAUUU	AAAUUUCCAGAUUUGCUUGGG
DHRS12-2	CUCCAUGUUCUGAUCAAUAAU	AUUAUUGAUCAGAACAUGGAG
DHRS12-3	GCAGGUUGCAUGGUCAAUAAA	UUUAUUGACCAUGCAACCUGC
DHRS1-3	CCAGGAAGCCUGCAGUAUAUG	CAUAUACUGCAGGCUUCCUGG
DHRS13-1	CCCUCAGAGCUCACCAGAUUU	AAAUCUGGUGAGCUCUGAGGG
DHRS13-2	UGGACAUCCUCAUCCACAAUG	CAUUGUGGAUGAGGAUGUCCA
DHRS13-3	AGCUGGCUAAUGUACUGUUUG	CAAACAGUACAUUAGCCAGCU
DHRS2-1	CUCUUCCAUUGCAGCUUAUAA	UUAUAAGCUGCAAUGGAAGAG
DHRS2-2	CUGCGUGGUUCCAGGAAUUAU	AUAAUUCCUGGAACCACGCAG
DHRS2-3	AUCAUCAGCUGCAGAGGAUUG	CAAUCCUCUGCAGCUGAUGAU
DHRS3-1	UCCCUCUACAGAUGAUCUAUC	GAUAGAUCAUCUGUAGAGGGA
DHRS3-2	GUAUGCUGGAGCUGCAGAAUG	CAUUCUGCAGCUCCAGCAUAC
DHRS3-3	ACUUUCAAAGGGCGGACAUAG	CUAUGUCCGCCCUUUGAAAGU
DHRS4-1	GACAAGACUCUGGACAUUAAU	AUUAAUGUCCAGAGUCUUGUC
DHRS4-2	CCUUUCUUUGGAAGCAUAAUG	CAUUAUGCUUCCAAAGAAAGG
DHRS4-3	CUGCCUAGCACCUGGACUUAU	AUAAGUCCAGGUGCUAGGCAG
DHRS4L2-1	GACAAGACUCUGGACAUUAAU	AUUAAUGUCCAGAGUCUUGUC
DHRS4L2-2	AGUCCUUACAAUGUCAGUAAA	UUUACUGACAUUGUAAGGACU
DHRS4L2-3	ACUGCCUGCACCUGGACUUAU	AUAAGUCCAGGUGCAGGCAGU
DHRS7-1	UGCCUAGAGAAUGGCAAUUUA	UAAAUUGCCAUUCUCUAGGCA
DHRS7-2	UGCCACAUACCCAGGUAUAAU	AUUAUACCUGGGUAUGUGGCA

DHRS7-3	GGAUGCAGACUCUUCUUAUUU	AAAUAAGAAGAGUCUGCAUCC
DHRS7B-1	CGAGAUGGAACAGUAUGAAAU	AUUUCAUACUGUUCCAUCUCG
DHRS7B-2	CACACCAACCUCUCUGUAAAU	AUUUACAGAGAGGUUGGUGUG
DHRS7B-3	UGCCUUCCUUGGCUGUUUAUC	GAUAAACAGCCAAGGAAGGCA
DHRS7C-1	CAAAUCGUGUUAGUGAAUAAU	AUUAUUCACUAACACGAUUUG
DHRS7C-2	CAGCGGCCUCCUCUUCAUUUA	UAAAUGAAGAGGAGGCCGCUG
DHRS7C-3	GGAAGAAGCAAGAGGUGUUUA	UAAACACCUCUUGCUUCUUCC
DHRS9-1	AUCAGGAUCAACAGCUUUAAA	UUUAAAGCUGUUGAUCCUGAU
DHRS9-2	AGCUCAAGGGAGAGUUAUUAA	UUAAUAACUCUCCCUUGAGCU
DHRS9-3	ACAAACUGAAAGGCAAUAAAU	AUUUAUUGCCUUUCAGUUUGU
DHRSX-1	UGUUAUCAUAGCUGGAAAUAA	UUAUUUCCAGCUAUGAUAACA
DHRSX-2	GAGACUUGGCAUGCAUGUUAU	AUAACAUGCAUGCCAAGUCUC
DHRSX-3	AGAUGGAUUCGAAGAACAUUU	AAAUGUUCUUCGAAUCCAUCU
DHTKD1-1	CCAGGUUGGUGACAGUAUAUU	AAUAUACUGUCACCAACCUGG
DHTKD1-2	AUAGAGGGAGGCUGAAUUUAU	AUAAAUUCAGCCUCCCUCUAU
DHTKD1-3	GGAGGAGGUGUCUGAAAUAAA	UUUAUUUCAGACACCUCCUCC
DLD-1	GGAUAUGUUGCUGCUAUUAAA	UUUAAUAGCAGCAACAUAUCC
DLD-2	UCCGAAGUUCGCUUGAAUUUA	UAAAUUCAAGCGAACUUCGGA
DLD-3	UACAGGUGCUUUAUCUUUAAA	UUUAAAGAUAAAGCACCUGUA
DMGDH-1	AGAGCAGAAACAGUGAUAAUU	AAUUAUCACUGUUUCUGCUCU
DMGDH-2	GACCUGGAAGGAUCAUAUUAU	AUAAUAUGAUCCUUCCAGGUC
DMGDH-3	GGAAGCUGGACUGGAAUAUUU	AAAUAUUCCAGUCCAGCUUCC
DPYD-1	CCUGAUAAGAACUGCUUUAAU	AUUAAAGCAGUUCUUAUCAGG
DPYD-2	GUGUAGGUGGAUGCAAUUUAU	AUAAAUUGCAUCCACCUACAC
DPYD-3	GGUUUGCCAGAACCCAAUAAA	UUUAUUGGGUUCUGGCAAACC
EHHADH-1	UGUGGAGCAGAGGGCAAAUUU	AAAUUUGCCCUCUGCUCCACA
EHHADH-2	CGCUGAAAGGAAAGCAAAUAA	UUAUUUGCUUUCCUUUCAGCG
EHHADH-3	UCCUUGAACGCUGCUUAUAUU	AAUAUAAGCAGCGUUCAAGGA
ETFDH-1	CCAGGGCUUCCAAUGAAUAAU	AUUAUUCAUUGGAAGCCCUGG
ETFDH-2	UCUAGCCAAGCAACUAUAUAA	UUAUAUAGUUGCUUGGCUAGA
ETFDH-3	AUGACAGUAUACCUGUAAAUA	UAUUUACAGGUAUACUGUCAU
G6PD-1	AUCAGUCGGAUACACACAUAU	AUAUGUGUGUAUCCGACUGAU
G6PD-2	AGAAGGUCAAGGUGUUGAAAU	AUUUCAACACCUUGACCUUCU
G6PD-3	GCCUCAACAGCCACAUGAAUG	CAUUCAUGUGGCUGUUGAGGC
GAPDH-1	ACUCUGGUAAAGUGGAUAUUG	CAAUAUCCACUUUACCAGAGU
GAPDH-2	GAUUCCACCCAUGGCAAAUUC	GAAUUUGCCAUGGGUGGAAUC
GAPDH-3	CCUGGUAUGACAACGAAUUUG	CAAAUUCGUUGUCAUACCAGG
GAPDHS-1	CACCAGUCAGGGAGGAAAUAA	UUAUUUCCUCCCUGACUGGUG
GAPDHS-2	CUGCAUGGAGAAGGGUGUUAA	UUAACACCCUUCUCCAUGCAG
GAPDHS-3	ACAAUUUCGUGAAGCUCAUUU	AAAUGAGCUUCACGAAAUUGU
GCDH-1	CAGACAUGCUCACUGAGAUUA	UAAUCUCAGUGAGCAUGUCUG
GCDH-2	UUCUCUGCUGAAGAGGAAUAA	UUAUUCCUCUUCAGCAGAGAA
GCDH-3	UCGUCAUGCACCCUAUCUAUG	CAUAGAUAGGGUGCAUGACGA

GLUD1-1	AUAGGGCACUAUGAUAUUAAU	AUUAAUAUCAUAGUGCCCUAU
GLUD1-2	CCUACACUCUAUGAGAUAUUU	AAAUAUCUCAUAGAGUGUAGG
GLUD1-3	AGCGUUCUGCCAGGCAAAUUA	UAAUUUGCCUGGCAGAACGCU
GPD1-1	CCACUGGCAUAUCUCUUAUUA	UAAUAAGAGAUAUGCCAGUGG
GPD1-2	CGGGUGACCAUGUGGGUAUUU	AAAUACCCACAUGGUCACCCG
GPD1-3	GAGAUCUGUGGAGCCUUAAAG	CUUUAAGGCUCCACAGAUCUC
GPD1L-1	GUCAAGAAACUUCAGAAAUUU	AAAUUUCUGAAGUUUCUUGAC
GPD1L-2	ACUGACAGACAUCAUAAAUAA	UUAUUUAUGAUGUCUGUCAGU
GPD1L-3	ACUUCUGCAGACUCCAAAUUU	AAAUUUGGAGUCUGCAGAAGU
GPD2-1	CAGCAGCAGAAGCACUAAAUU	AAUUUAGUGCUUCUGCUGCUG
GPD2-2	UCAGUGAGAGUGGCCUUAUUA	UAAUAAGGCCACUCUCACUGA
GPD2-3	GCAGACCAGAAAGGCUUUAUU	AAUAAAGCCUUUCUGGUCUGC
H6PD-1	GCACCCAGGCAUGUGGAAUAU	AUAUUCCACAUGCCUGGGUGC
H6PD-2	ACCUGGCUAAGAAGUACUUAU	AUAAGUACUUCUUAGCCAGGU
H6PD-3	UUCCAUGGCCGGAAGAAUUUC	GAAAUUCUUCCGGCCAUGGAA
HADH-1	AUUGACACUGCUAUGAAAUUA	UAAUUUCAUAGCAGUGUCAAU
HADH-2	GCCCAGCCCAUCCUUAAAUAA	UUAUUUAAGGAUGGGCUGGGC
HADH-3	GCCUCGGCCAAGAAGAUAAUC	GAUUAUCUUCUUGGCCGAGGC
HADHA-1	UCCGCUCCCGAGGUUAUAUAU	AUAUAUAACCUCGGGAGCGGA
HADHA-2	CUCUGUGAAUCUCAGAAAUUU	AAAUUUCUGAGAUUCACAGAG
HADHA-3	GUGGACCGGCUCAAGAAAUAU	AUAUUUCUUGAGCCGGUCCAC
HADHB-1	ACGUUAGCCAAACCCAAUAUA	UAUAUUGGGUUUGGCUAACGU
HADHB-2	GGGCCAGCGACUGUCUUUAAU	AUUAAAGACAGUCGCUGGCCC
HADHB-3	UCCUUUGGAGAAGUUUAAUAA	UUAUUAAACUUCUCCAAAGGA
HIBADH-1	ACAUGGCUAUCCACUUAUUAU	AUAAUAAGUGGAUAGCCAUGU
HIBADH-2	GUGAAGAAGGGCUCAUUAUUA	UAAUAAUGAGCCCUUCUUCAC
HIBADH-3	UGGCGUUCCUCGGCUAAUAA	UUAUUAGCCGAGGGAACGCCA
HPGD-1	UUGCACAGCAGCCGGUUUAUU	AAUAAACCGGCUGCUGUGCAA
HPGD-2	CAUUGAAGAUGAUGCUUUAAA	UUUAAAGCAUCAUCUUCAAUG
HPGD-3	UGCUUUAAAUGGUGCUAUUAU	AUAAUAGCACCAUUUAAAGCA
HSD11B1-1	CCUCCAUCAGAAAGGAAUAUU	AAUAUUCCUUUCUGAUGGAGG
HSD11B1-2	CGCCAAGAAGAAGUGUAUUAU	AUAAUACACUUCUUCUUGGCG
HSD11B1-3	CUACUCAACGAGCUAUAAUAU	AUAUUAUAGCUCGUUGAGUAG
HSD11B1L-1	GCCCUGUUCUUCGCCUAUUAU	AUAAUAGGCGAAGAACAGGGC
HSD11B1L-2	GGCCCUGUUCUUCGCCUAUUA	UAAUAGGCGAAGAACAGGGCC
HSD11B1L-3	GGCUCAUGCAGGUAAACUUUG	CAAAGUUUACCUGCAUGAGCC
HSD11B2-1	UGACCAAACCAGGAGACAUUA	UAAUGUCUCCUGGUUUGGUCA
HSD11B2-2	UAGCUGCAUGGAGGUGAAUUU	AAAUUCACCUCCAUGCAGCUA
HSD11B2-3	AGCUGCAUGGAGGUGAAUUUC	GAAAUUCACCUCCAUGCAGCU
HSD17B10-1	CUAGCAAGACGUACAACUUAA	UUAAGUUGUACGUCUUGCUAG
HSD17B10-2	UAGCAAGACGUACAACUUAAA	UUUAAGUUGUACGUCUUGCUA
HSD17B10-3	AGCAAGACGUACAACUUAAAG	CUUUAAGUUGUACGUCUUGCU
HSD17B1-1	AUCCAUCCCAGAGCUUCAAAG	CUUUGAAGCUCUGGGAUGGAU

HSD17B11-1	GCUGCCUUUCAAUGACGUUUA	UAAACGUCAUUGAAAGGCAGC
HSD17B11-2	CCCACAGCAAGCAAGUCUUUC	GAAAGACUUGCUUGCUGUGGG
HSD17B11-3	AGCUGGUUCUCUGGGAUAUAA	UUAUAUCCCAGAGAACCAGCU
HSD17B1-2	GCAGCAACCGAGAAGAUAUUU	AAAUAUCUUCUCGGUUGCUGC
HSD17B12-1	GAUGCAGUUAUUGGAUAUAAA	UUUAUAUCCAAUAACUGCAUC
HSD17B12-2	ACCAGGUUUCCAGUGAAAUAA	UUAUUUCACUGGAAACCUGGU
HSD17B12-3	CUUUGCAUCAGAAGAUAUUUA	UAAAUAUCUUCUGAUGCAAAG
HSD17B1-3	ACCUGCCUUCUUGGAUUUAUU	AAUAAAUCCAAGAAGGCAGGU
HSD17B13-1	UAUUGGUUCUGUGGGAUAUUA	UAAUAUCCCACAGAACCAAUA
HSD17B13-2	GUAACAAUCGUGGUGAAUAAU	AUUAUUCACCACGAUUGUUAC
HSD17B13-3	CCAUAUUGUUCCAGCAAAUUU	AAAUUUGCUGGAACAAUAUGG
HSD17B14-1	GCUCCCUGGAGCUGUCUUUAU	AUAAAGACAGCUCCAGGGAGC
HSD17B14-2	UCUGAGACCAUCCGCCGAUUU	AAAUCGGCGGAUGGUCUCAGA
HSD17B14-3	AGCUUUGGCCCUGGAUGAAAG	CUUUCAUCCAGGGCCAAAGCU
HSD17B2-1	UGGAGGCUUCCUAACAAAUAU	AUAUUUGUUAGGAAGCCUCCA
HSD17B2-2	UAUUUGCCUAUUGGCAUAUAU	AUAUAUGCCAAUAGGCAAAUA
HSD17B2-3	AGUACUAUGUGGGACAGUAUU	AAUACUGUCCCACAUAGUACU
HSD17B3-1	GACUCAAUGUUGUCCUUAUUA	UAAUAAGGACAACAUUGAGUC
HSD17B3-2	GACAUCUACGAGCAUAUUAAA	UUUAAUAUGCUCGUAGAUGUC
HSD17B3-3	GCCCUGCAAGAGGAAUAUAAA	UUUAUAUUCCUCUUGCAGGGC
HSD17B4-1	GUGAUGAAGACUGGGAUAUAA	UUAUAUCCCAGUCUUCAUCAC
HSD17B4-2	UACGGAACUGGAAGCUAUUAU	AUAAUAGCUUCCAGUUCCGUA
HSD17B4-3	UAUAACCAAAGGCGGAAAUAU	AUAUUUCCGCCUUUGGUUAUA
HSD17B6-1	AGCUGGCUGGGAUGCUAAAUU	AAUUUAGCAUCCCAGCCAGCU
HSD17B6-2	GCUGGCUGGGAUGCUAAAUUU	AAAUUUAGCAUCCCAGCCAGC
HSD17B6-3	UUCAUCCCUCUAUCUUAUUUA	UAAAUAAGAUAGAGGGAUGAA
HSD17B7-1	UCAGAGAUUAGACUGUAUAUA	UAUAUACAGUCUAAUCUCUGA
HSD17B7-2	CCCUACAGCUCUUCCAAAUAU	AUAUUUGGAAGAGCUGUAGGG
HSD17B7-3	CUCAAUCCUCUGAUCAAAUAU	AUAUUUGAUCAGAGGAUUGAG
HSD17B8-1	AGAAAGUGGUGGACAAGAUUA	UAAUCUUGUCCACCACUUUCU
HSD17B8-2	GGUGGACAAGAUUACUGAAAU	AUUUCAGUAAUCUUGUCCACC
HSD17B8-3	CUGAGGAUGACUGGGACAAAG	CUUUGUCCCAGUCAUCCUCAG
HSD3B1-1	AUUCCUUUCUGCUAGUAUAAA	UUUAUACUAGCAGAAAGGAAU
HSD3B1-2	CUUCCUACUCAGGCCAAUUUA	UAAAUUGGCCUGAGUAGGAAG
HSD3B1-3	CGUAUUCACCUUCUCUUAUAA	UUAUAAGAGAAGGUGAAUACG
HSD3B2-1	UGCGUUAAGACCCACAUAUAU	AUAUAUGUGGGUCUUAACGCA
HSD3B2-2	UUCCUUUCUGCCAGUAUAAAU	AUUUAUACUGGCAGAAAGGAA
HSD3B2-3	CUUCCUACUCAGCCCAAUUUA	UAAAUUGGGCUGAGUAGGAAG
HSD3B7-1	CUACAGGAGCUACGAGGAUUU	AAAUCCUCGUAGCUCCUGUAG
HSD3B7-2	CGGGUCUAUGUGGGCAAUGUU	AACAUUGCCCACAUAGACCCG
HSD3B7-3	UACAGGAGCUACGAGGAUUUC	GAAAUCCUCGUAGCUCCUGUA
HSDL1-1	GCAAGCCGAGGUCUCAAUAUA	UAUAUUGAGACCUCGGCUUGC
HSDL1-2	ACGUUGGCAUCUUGGUAAAUA	UAUUUACCAAGAUGCCAACGU

HSDL1-3	UCUGCUUCUAAGGCUUAUUUA	UAAAUAAGCCUUAGAAGCAGA
HSDL2-1	AGCAAAGGAUGGAGCAAAUAU	AUAUUUGCUCCAUCCUUUGCU
HSDL2-2	UUGGAAUGGCAGAAGAAUUUA	UAAAUUCUUCUGCCAUUCCAA
HSDL2-3	UCAGGGAAAUUGAAGAUUAAA	UUUAAUCUUCAAUUUCCCUGA
IDH1-1	GGAUGCUGCAGAAGCUAUAAA	UUUAUAGCUUCUGCAGCAUCC
IDH1-2	GACAUCUUUCAGGAGAUAUAU	AUAUAUCUCCUGAAAGAUGUC
IDH1-3	GCAAAGCUUGAUAACAAUAAA	UUUAUUGUUAUCAAGCUUUGC
IDH2-1	UGAUGAGAUGACCCGUAUUAU	AUAAUACGGGUCAUCUCAUCA
IDH2-2	GGACAUCCAGCUAAAGUAUUU	AAAUACUUUAGCUGGAUGUCC
IDH2-3	AUCUUUGACAAGCACUAUAAG	CUUAUAGUGCUUGUCAAAGAU
IDH3A-1	UGUUCAGACAGUAACUUUAAU	AUUAAAGUUACUGUCUGAACA
IDH3A-2	GGUCACCCAUCUAUGAAUUUA	UAAAUUCAUAGAUGGGUGACC
IDH3A-3	CAGAAAGCUGUAAAGAUAUUA	UAAUAUCUUUACAGCUUUCUG
IDH3B-1	AGGCGUAAGUUGGACUUAUUU	AAAUAAGUCCAACUUACGCCU
IDH3B-2	CAGGCAGUGGGCAGGAAUAUA	UAUAUUCCUGCCCACUGCCUG
IDH3B-3	ACCUGAGUGAGGUGCAGAAUA	UAUUCUGCACCUCACUCAGGU
IDH3G-1	CGGCAAGAGUAUCGCCAAUAA	UUAUUGGCGAUACUCUUGCCG
IDH3G-2	CAUCCAUGGACAAUGAGAAUA	UAUUCUCAUUGUCCAUGGAUG
IDH3G-3	UCCAUGGACAAUGAGAAUAUG	CAUAUUCUCAUUGUCCAUGGA
IMPDH1-1	GCACCCGUGAGGAUGACAAAU	AUUUGUCAUCCUCACGGGUGC
IMPDH1-2	CACCCGUGAGGAUGACAAAUA	UAUUUGUCAUCCUCACGGGUG
IMPDH1-3	ACCCGUGAGGAUGACAAAUAC	GUAUUUGUCAUCCUCACGGGU
IMPDH2-1	GUUCGGAAAGUGAAGAAAUAU	AUAUUUCUUCACUUUCCGAAC
IMPDH2-2	GGGAUCCGGCUAAAGAAAUAU	AUAUUUCUUUAGCCGGAUCCC
IMPDH2-3	CAGCAGCCAGAACAGAUAUUU	AAAUAUCUGUUCUGGCUGCUG
IVD-1	UUCAAGAACCUGCGAGAAUUU	AAAUUCUCGCAGGUUCUUGAA
IVD-2	ACAUCCUGGGCCAUGAGAAUA	UAUUCUCAUGGCCCAGGAUGU
IVD-3	CUGUGCAGGUGUGAUUCUUUA	UAAAGAAUCACACCUGCACAG
L2HGDH-1	UGUCAUACAUAGUGGAAUUUA	UAAAUUCCACUAUGUAUGACA
L2HGDH-2	AGUCUCUGAAAGCCAAAUUAU	AUAAUUUGGCUUUCAGAGACU
L2HGDH-3	CCACAGAUGUUAUGGAUAUAA	UUAUAUCCAUAACAUCUGUGG
LDHA-1	UAAAGGAUCAGCUGAUUUAUA	UAUAAAUCAGCUGAUCCUUUA
LDHA-2	GGGAGAAAGCCGUCUUAAUUU	AAAUUAAGACGGCUUUCUCCC
LDHA-3	UAAGGGUCUUUACGGAAUAAA	UUUAUUCCGUAAAGACCCUUA
LDHAL6A-1	UGUGCUAUCAGCAUCUUAUUA	UAAUAAGAUGCUGAUAGCACA
LDHAL6A-2	CGAAAUGUAUCCAUCUUUAAA	UUUAAAGAUGGAUACAUUUCG
LDHAL6A-3	UAAGGGCCUCUAUGGAAUAAA	UUUAUUCCAUAGAGGCCCUUA
LDHAL6B-1	GCGCUAUCAGCAUCUUAUUAA	UUAAUAAGAUGCUGAUAGCGC
LDHAL6B-2	GGAGAAACGCGCCUUAAUUUA	UAAAUUAAGGCGCGUUUCUCC
LDHAL6B-3	UCCAGUUUCCACCAUAAUUAA	UUAAUUAUGGUGGAAACUGGA
LDHB-1	CUGCAGCAUGGGAGCUUAUUU	AAAUAAGCUCCCAUGCUGCAG
LDHB-2	UUGUGGCAGAUAAAGAUUAUU	AAUAAUCUUUAUCUGCCACAA
LDHB-3	AGUCCUGAUUGCAUCAUAAUU	AAUUAUGAUGCAAUCAGGACU

LDHC-1	CCAACGUAAUGUGGCUAUAAU	AUUAUAGCCACAUUACGUUGG
LDHC-2	AGCUGCCAUGGUUGGAUUAUU	AAUAAUCCAACCAUGGCAGCU
LDHC-3	CACCAUGGUUAAGGGAUUAUA	UAUAAUCCCUUAACCAUGGUG
LDHD-1	CUUCGGCUUCUGGCCAGAAAU	AUUUCUGGCCAGAAGCCGAAG
LDHD-2	CAGGUACAGCAAGCUGAAUUG	CAAUUCAGCUUGCUGUACCUG
LDHD-3	AGACCAAGGAGGAUCUGAAUG	CAUUCAGAUCCUCCUUGGUCU
MDH1-1	UGGUAAAGAUCAGCCUAUAAU	AUUAUAGGCUGAUCUUUACCA
MDH1-2	AGGGUGCAGCCUUAGAUAAAU	AUUUAUCUAAGGCUGCACCCU
MDH1-3	UGUUGAAGGUCUCCCUAUUAA	UUAAUAGGGAGACCUUCAACA
MDH2-1	UCAUUGCCAAUCCGGUUAAUU	AAUUAACCGGAUUGGCAAUGA
MDH2-2	AGGUUGUGAUGUGGUAGUUAU	AUAACUACCACAUCACAACCU
MDH2-3	CCGCCUGACCCUCUAUGAUAU	AUAUCAUAGAGGGUCAGGCGG
MTHFD1-1	CACACCACGCCUGGCAAUAUU	AAUAUUGCCAGGCGUGGUGUG
MTHFD1-2	UCUGGAUGAGGAGGUAAAUAA	UUAUUUACCUCCUCAUCCAGA
MTHFD1-3	UGUCUGAAGAGGUAGAAUUAU	AUAAUUCUACCUCUUCAGACA
MTHFD1L-1	CAAGCCGGUUCUUGCAAUUAU	AUAAUUGCAAGAACCGGCUUG
MTHFD1L-2	AGCAGUGAAGCCGAGAUUAUA	UAUAAUCUCGGCUUCACUGCU
MTHFD1L-3	AGAAGAGGAAGUGAGUAAAUU	AAUUUACUCACUUCCUCUUCU
MTHFD2-1	GAGGAAGAAUUGUUGAAUUUA	UAAAUUCAACAAUUCUUCCUC
MTHFD2-2	GAUGGCUUUCAUGUAAUUAAU	AUUAAUUACAUGAAAGCCAUC
MTHFD2-3	UCAUUGAUGUGGGAAUAAAUA	UAUUUAUUCCCACAUCAAUGA
MTHFD2L-1	GACCUCACCUCAGUAUAAUUU	AAAUUAUACUGAGGUGAGGUC
MTHFD2L-2	CCAAGAGUCAGCGGUAUAUUA	UAAUAUACCGCUGACUCUUGG
MTHFD2L-3	AUACGCAGCUGGCAGAUAUUA	UAAUAUCUGCCAGCUGCGUAU
NQO1-1	CGAGUCUGUUCUGGCUUAUAA	UUAUAAGCCAGAACAGACUCG
NQO1-2	GAGUCUGUUCUGGCUUAUAAA	UUUAUAAGCCAGAACAGACUC
NQO1-3	AGAAACGCCUGGAGAAUAUUU	AAAUAUUCUCCAGGCGUUUCU
NSDHL-1	AUCCUGACAGGCCUCAAUUAU	AUAAUUGAGGCCUGUCAGGAU
NSDHL-2	AGGAUAUGCUGUCAAUGUAUU	AAUACAUUGACAGCAUAUCCU
NSDHL-3	CCCAGCUCUGAAAGGUGUAAA	UUUACACCUUUCAGAGCUGGG
OGDH-1	CUGAGUAUGAGGAGGAAAUUU	AAAUUUCCUCCUCAUACUCAG
OGDH-2	CAUUCCGGAAGCCGUUAAUUA	UAAUUAACGGCUUCCGGAAUG
OGDH-3	UGCACCGGCAAAGUGUAUUAU	AUAAUACACUUUGCCGGUGCA
OGDHL-1	GACCCAGAGGCUGUGAUAUAU	AUAUAUCACAGCCUCUGGGUC
OGDHL-2	CGGACCAAGACCAGCAAAUUG	CAAUUUGCUGGUCUUGGUCCG
OGDHL-3	UGAUCACAACCAUUGAUAAAC	GUUUAUCAAUGGUUGUGAUCA
PDHA1-1	GCUGGUAGCAUCCCGUAAUUU	AAAUUACGGGAUGCUACCAGC
PDHA1-2	UGAGGUCUGCCUGACUUUAUA	UAUAAAGUCAGGCAGACCUCA
PDHA1-3	AUGGCAGCUUUGUGGAAAUUA	UAAUUUCCACAAAGCUGCCAU
PDHA2-1	UGACGCUACAUUUGAAAUUAA	UUAAUUUCAAAUGUAGCGUCA
PDHA2-2	GCUCUGGCCUGUAAAUAUAAA	UUUAUAUUUACAGGCCAGAGC
PDHA2-3	GUAAGAGGGAUCCUAUAAUAA	UUAUUAUAGGAUCCCUCUUAC
PDHB-1	ACAGUUCGUGAUGCUAUAAAU	AUUUAUAGCAUCACGAACUGU

PDHB-2	AGGAUGCUAAAGGACUUAUUA	UAAUAAGUCCUUUAGCAUCCU
PDHB-3	UGAAUGUGAGGUGAUAAAUAU	AUAUUUAUCACCUCACAUUCA
PDHX-1	AGUCCAGCUGCCCGCAAUAUU	AAUAUUGCGGGCAGCUGGACU
PDHX-2	CUGGUCAAAGAUGACAUUAAA	UUUAAUGUCAUCUUUGACCAG
PDHX-3	CCAAAGCAACUGCCAUUUAUU	AAUAAAUGGCAGUUGCUUUGG
PDK1-1	GCCUGUCAGACUGGCAAAUAU	AUAUUUGCCAGUCUGACAGGC
PDK1-2	UGAGGAUGCUAAAGCUAUUUA	UAAAUAGCUUUAGCAUCCUCA
PDK1-3	CGUCUGUGUGAUUUGUAUUAU	AUAAUACAAAUCACACAGACG
PDK2-1	AGCUCCUGUGUGACAAGUAUU	AAUACUUGUCACACAGGAGCU
PDK2-2	GCUCCUGUGUGACAAGUAUUA	UAAUACUUGUCACACAGGAGC
PDK2-3	CUCCUGUGUGACAAGUAUUAC	GUAAUACUUGUCACACAGGAG
PDK3-1	UUAAUCUUCUGCCGGAUAAUU	AAUUAUCCGGCAGAAGAUUAA
PDK3-2	CUCUUUCCGCAUGCUUAUUAA	UUAAUAAGCAUGCGGAAAGAG
PDK3-3	GUACUGAUGCUGUCAUUUAUU	AAUAAAUGACAGCAUCAGUAC
PDK4-1	UCCCGACCCAAUUAGUAAAUA	UAUUUACUAAUUGGGUCGGGA
PDK4-2	ACCAGCACAUUCUUAUAUUUA	UAAAUAUAAGAAUGUGCUGGU
PDK4-3	CUCUGUGAUCAGUAUUAUUUA	UAAAUAAUACUGAUCACAGAG
PDPR-1	GGAUGCUGAUGGAAGAAUUUA	UAAAUUCUUCCAUCAGCAUCC
PDPR-2	GCUGAUGGAAGAAUUUAUAUU	AAUAUAAAUUCUUCCAUCAGC
PDPR-3	CGAGAGUCUCGGGUGAAAUUA	UAAUUUCACCCGAGACUCUCG
PGD-1	ACGGAGGAAAUUCUGAAUAUA	UAUAUUCAGAAUUUCCUCCGU
PGD-2	AUUGAAAUCACAGCCAAUAUU	AAUAUUGGCUGUGAUUUCAAU
PGD-3	UUUGGCUGGACUCUCAAUUAU	AUAAUUGAGAGUCCAGCCAAA
PHGDH-1	CCUUCCGGGACCAAGAAAUUA	UAAUUUCUUGGUCCCGGAAGG
PHGDH-2	UCUGGACCAGCUUUGUUUAAA	UUUAAACAAAGCUGGUCCAGA
PHGDH-3	GGUGAAAUGCUGUGGUUUAAA	UUUAAACCACAGCAUUUCACC
PRODH-1	GGAUGGCAGUGGCACGAAUAA	UUAUUCGUGCCACUGCCAUCC
PRODH-2	UGACGGCUUCAUAGCCAUUAA	UUAAUGGCUAUGAAGCCGUCA
PRODH2-1	GACGGCUUCAUAGCCAUUAAG	CUUAAUGGCUAUGAAGCCGUC
PRODH2-2	CACCUACCAGGCCUGUCUAAA	UUUAGACAGGCCUGGUAGGUG
PRODH2-3	GCCGGCUAUGUAGUGUAUAAG	CUUAUACACUACAUAGCCGGC
PRODH-3	UUCUCCGAGCAUCCGUCUAUG	CAUAGACGGAUGCUCGGAGAA
RDH10-1	GUCUCAGUCCUGGUCAAUAAU	AUUAUUGACCAGGACUGAGAC
RDH10-2	CCUACGAUGCUGGAGAUUAAU	AUUAAUCUCCAGCAUCGUAGG
RDH10-3	UGGGAAUGGUGAGGAAGAAAU	AUUUCUUCCUCACCAUUCCCA
RDH11-1	CUGCCCUUCCUUCUGUAUAUG	CAUAUACAGAAGGAAGGGCAG
RDH11-2	CUGUCUGAUACUAAGUCUAUU	AAUAGACUUAGUAUCAGACAG
RDH11-3	UAACCUGCAGGGCGAGAAAUU	AAUUUCUCGCCCUGCAGGUUA
RDH12-1	CGAGGAGCCCGAGUCUAUAUU	AAUAUAGACUCGGGCUCCUCG
RDH12-2	CCUUCUUCUCGUUCCUGUAUA	UAUACAGGAACGAGAAGAAGG
RDH12-3	GGUGGAGUGUGUAGAACAAAU	AUUUGUUCUACACACUCCACC
RDH13-1	GGAGCGAGUGGACAUUCUAAU	AUUAGAAUGUCCACUCGCUCC
RDH13-2	ACUGGCAGACGAGGAAGUAUA	UAUACUUCCUCGUCUGCCAGU

RDH13-3	UGGCAGACGAGGAAGUAUAAC	GUUAUACUUCCUCGUCUGCCA
RDH14-1	ACAGUGAACAAAGCUAUAAUA	UAUUAUAGCUUUGUUCACUGU
RDH14-2	GGUGCCCAGACUUCCAUUUAU	AUAAAUGGAAGUCUGGGCACC
RDH14-3	UGCCCAGACUUCCAUUUAUUU	AAAUAAAUGGAAGUCUGGGCA
RDH16-1	GCUGAGCCACCUGAGAGAUAA	UUAUCUCUCAGGUGGCUCAGC
RDH16-2	CAGUAAGGAGAGAUUCUUAAA	UUUAAGAAUCUCUCCUUACUG
RDH16-3	UAAGAAAUCAGCUGAACAAAU	AUUUGUUCAGCUGAUUUCUUA
RDH5-1	GGCUACUGUGUCUCCAAAUUU	AAAUUUGGAGACACAGUAGCC
RDH5-2	GAGGCGGGAUGUAGCUCAUUU	AAAUGAGCUACAUCCCGCCUC
RDH5-3	GCUACUGUGUCUCCAAAUUUG	CAAAUUUGGAGACACAGUAGC
RDH8-1	GUGGACGUGCUGGUGAAUAAU	AUUAUUCACCAGCACGUCCAC
RDH8-2	UGGACGUGCUGGUGAAUAAUG	CAUUAUUCACCAGCACGUCCA
RDH8-3	CUGCCAUGCAGAAUGUCUUUG	CAAAGACAUUCUGCAUGGCAG
SARDH-1	UCGUGUGUGGACGGAUGAUUU	AAAUCAUCCGUCCACACACGA
SARDH-2	CCGAGAAGAGUGUGCCAUAUC	GAUAUGGCACACUCUUCUCGG
SARDH-3	AGGAGGUGUCAGACAAGUUUG	CAAACUUGUCUGACACCUCCU
SDHA-1	CUUUCUGAGGCAGGGUUUAAU	AUUAAACCCUGCCUCAGAAAG
SDHA-2	UCGCUAUUGCACACCUUAUAU	AUAUAAGGUGUGCAAUAGCGA
SDHA-3	AGAUAAAGUCCUCCAAUUAA	UUAAUUGGAGGGACUUUAUCU
SDHAF1-1	GAGGCAGGUUCUGAGCCUGUA	UACAGGCUCAGAACCUGCCUC
SDHAF1-2	UCUGAGCCUGUACCGCGAUCU	AGAUCGCGGUACAGGCUCAGA
SDHAF1-3	CUGCGCAUCGAGUACCUGUAC	GUACAGGUACUCGAUGCGCAG
SDHAF2-1	UAGUAAUGACUGGGAUAUUUA	UAAAUAUCCCAGUCAUUACUA
SDHAF2-2	CCUCUAUGACCGCCUGAUUAA	UUAAUCAGGCGGUCAUAGAGG
SDHAF2-3	AGUAAUGACUGGGAUAUUUAC	GUAAAUAUCCCAGUCAUUACU
SDHAF3-1	AGUACGUGAAAGACGAAUUUA	UAAAUUCGUCUUUCACGUACU
SDHAF3-2	AGACGAAUUUAGGAGACAUAA	UUAUGUCUCCUAAAUUCGUCU
SDHAF3-3	UGACUUUCGUGAUGAACAAAU	AUUUGUUCAUCACGAAAGUCA
SDHAF4-1	GCACCAGAGGAUUCCCAUUUA	UAAAUGGGAAUCCUCUGGUGC
SDHAF4-2	GAAAGUCUGAACUUGUCAAAC	GUUUGACAAGUUCAGACUUUC
SDHAF4-3	ACCUACCCGAUAUGGAGAUUG	CAAUCUCCAUAUCGGGUAGGU
SDHB-1	CUUAUGAAGUUGACCUUAAUA	UAUUAAGGUCAACUUCAUAAG
SDHB-2	CAUGGUAUUGGAUGCUUUAAU	AUUAAAGCAUCCAAUACCAUG
SDHB-3	CAAAUCCAUUGAGCCUUAUUU	AAAUAAGGCUCAAUGGAUUUG
SDHC-1	CGGUUCUGGAAUAAGAAUAUA	UAUAUUCUUAUUCCAGAACCG
SDHC-2	UGGGAACUUUGAGUCUUAUUU	AAAUAAGACUCAAAGUUCCCA
SDHC-3	CCUCAGCUCUGUAUCAGAAAU	AUUUCUGAUACAGAGCUGAGG
SDHD-1	UCUGCUUCCGGCUGCUUAUUU	AAAUAAGCAGCCGGAAGCAGA
SDHD-2	AGUGGUCAGACCUGCUCAUAU	AUAUGAGCAGGUCUGACCACU
SDHD-3	CUUGCUCUGCGAUGGACUAUU	AAUAGUCCAUCGCAGAGCAAG
SDR16C5-1	AGCACAUUUAUGGACUUAUAA	UUAUAAGUCCAUAAAUGUGCU
SDR16C5-2	GUCUUCUGGAGGCUAUGAUUU	AAAUCAUAGCCUCCAGAAGAC
SDR16C5-3	AGAACGUUGCUGGUGAAAUAG	CUAUUUCACCAGCAACGUUCU

SDR42E1-1	CCAGAAGGAAUCAAGUUUAUA	UAUAAACUUGAUUCCUUCUGG
SDR42E1-2	CAAGAAAGAGCUAGGUUAUAA	UUAUAACCUAGCUCUUUCUUG
SDR42E1-3	GAAGCAGUGGAAUGGUUUAAA	UUUAAACCAUUCCACUGCUUC
SDR9C7-1	CCUCACAGACCUCUCAUUUAU	AUAAAUGAGAGGUCUGUGAGG
SDR9C7-2	GACUUUGUGAAGGUGAUUAAU	AUUAAUCACCUUCACAAAGUC
SDR9C7-3	ACAGCUACGGAGAGGAUUAUU	AAUAAUCCUCUCCGUAGCUGU
SORD-1	GGAGGCCUUUGAAACAUUUAA	UUAAAUGUUUCAAAGGCCUCC
SORD-2	GUAUGGUCGAAUUGGGAAUUU	AAAUUCCCAAUUCGACCAUAC
SORD-3	GUCCAAGUCUGUGAAUGUAAA	UUUACAUUCACAGACUUGGAC
TDH-1	GACCAUCCACGAGUCUUAAUU	AAUUAAGACUCGUGGAUGGUC
TDH-2	CACAGUGGUCCAUUCAUUUAU	AUAAAUGAAUGGACCACUGUG
TDH-3	CUGGCGAGAGCAGUGAAUAUA	UAUAUUCACUGCUCUCGCCAG
UGDH-1	UUCUCCUACACUUCCUAUUUA	UAAAUAGGAAGUGUAGGAGAA
UGDH-2	AGAAGCUGAUCUUGUAUUUAU	AUAAAUACAAGAUCAGCUUCU
UGDH-3	GCAGCAGAUCUGAAGUAUAUU	AAUAUACUUCAGAUCUGCUGC
XDH-1	UGUGGAGGAGAUGGGAAUAAU	AUUAUUCCCAUCUCCUCCACA
XDH-2	CAGCCUCUCGCCAUCUUUAUU	AAUAAAGAUGGCGAGAGGCUG
XDH-3	GGAUCUCUCAGAGUAUUAU	AUAAUACUCUGAGAGAUCC
ZADH2-1	GAUCGUCCUAUCAACUAUAAA	UUUAUAGUUGAUAGGACGAUC
ZADH2-2	AUAUUCCGUGCUGUCAAUUAU	AUAAUUGACAGCACGGAAUAU
ZADH2-3	UAUUCCGUGCUGUCAAUUAUA	UAUAAUUGACAGCACGGAAUA
siRNA sequences against four acetyltransferases and HIF1A		
PCAF	GUUGGCUAUAUCAAGGAUUAU	AUAAUCCUUGAUAUAGCCAAC
TIP60	GGACGUAAGAACAAGAGUUAU	AUAACUCUUGUUCUUACGUCC
CBP	AUCGCCACGUCCCUUAGUAAC	GUUACUAAGGGACGUGGCGAU
p300	UAACCAAUGGUGGUGAUAUUA	UAAUAUCACCACCAUUGGUUA
HIF1A	CCGCUGGAGACACAAUCAUAU	AUAUGAUUGUGUCUCCAGCGG

Appendix Table S2. RT-qPCR primer sequences used in this study. Related to Methods.

RT-qPCR primer sequences (5'-3')		
Homo Target	Forward primer	Reverse primer
PCAF	AGGAAAACCTGTGGTTGAAGG	CAGTCTTCGTTGAGATGGTGC
TIP60	AACAAACGTCTGGATGAATGGG	AGGAAGTCCGTTCTTAGTGGG
CBP	CCTGCCACGTCACAGACTG	GGCCAGAGTTACTATTGAGGAGG
p300	GCTTCAGACAAGTCTTGGCAT	ACTACCAGATCGCAGCAATTC
HIF1A	ATCCATGTGACCATGAGGAAATG	TCGGCTAGTTAGGGTACACTTC
GLUT1	GGCCAAGAGTGTGCTAAAGAA	ACAGCGTTGATGCCAGACAG
HK1	CCAACATTCGTAAGGTCCATTCC	CCTCGGACTCCATGTGAACATT
PGK1	GAACAAGGTTAAAGCCGAGCC	GTGGCAGATTGACTCCTACCA
CCND1	TGGAGCCCGTGAAAAAGAGC	TCTCCTTCATCTTAGAGGCCAC
β-ACTIN	CACCATTGGCAATGAGCGGTTC	AGGTCTTTGCGGATGTCCACGT
Murine Target	Forward primer	Reverse primer
Tnfα	CCCTCACACTCAGATCATCT	GCTACGACGTGGGCTACAG
Ifng	ATGAACGCTACACACTGCATC	CCATCCTTTTGCCAGTTCCTC
Il6	TAGTCCTTCCTACCCCAATTTC	TTGGTCCTTAGCCACTCCTTC
Hif1a	GATGACGGCGACATGGTTTAC	CTCACTGGGCCATTTCTGTGT
β-Actin	GGCTGTATTCCCCTCCATCG	CCAGTTGGTAACAATGCCATGT